NASA TECHNICAL NOTE

NASA TN D-5124

c. 1

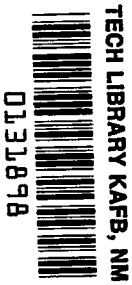

NASA TN D-5124

FILM BOILING FROM SUBMERGED SPHERES

by Robert C. Hendricks and Kenneth J. Baumeister

Lewis Research Center
Cleveland, Ohio

NATIONAL AERONAUTICS AND SPACE ADMINISTRATION • WASHINGTON, D. C. • JUNE 1969

FILM BOILING FROM SUBMERGED SPHERES

By Robert C. Hendricks and Kenneth J. Baumeister

Lewis Research Center
Cleveland, Ohio

NATIONAL AERONAUTICS AND SPACE ADMINISTRATION

For sale by the Clearinghouse for Federal Scientific and Technical Information
Springfield, Virginia 22151 – CFSTI price $3.00

ABSTRACT

The energy and momentum equations are solved analytically to predict the heat-transfer coefficient of small submerged spheres in film boiling. The analysis is based on the postulate that the rate of entropy production is maximized. In addition, the small-sphere theory is matched with the film-boiling correlation for flat plates to give a heat-transfer correlation which applies for large, as well as small, spheres.

Technical Film Supplement C-263 available on request.

FILM BOILING FROM SUBMERGED SPHERES

by Robert C. Hendricks and Kenneth J. Baumeister

Lewis Research Center

SUMMARY

The heat-transfer coefficient for pool film boiling from submerged spheres was analyzed. The model developed assumed a vapor dome on top of the sphere into which vapor flows from the thin-film vapor region which exists on the lower portion of the sphere.

In addition, the theoretical result for boiling from small spheres was matched with the heat-transfer coefficient from a flat plate to give a heat-transfer correlation that applies to both small and large spheres.

INTRODUCTION

Film boiling is one of the major mechanisms by which heat is transferred in cryogenic systems or wherever extremely high temperature differences are involved, as in quenching or spray cooling. Fundamental investigations into the phenomenon of film boiling have considered Leidenfrost boiling of liquid drops and film boiling from flat plates, wires, and spheres. This report is concerned with film boiling from submerged spheres of relatively small diameter and some of the similarities to film boiling from submerged cylinders.

Film boiling from horizontal wires (cylinders) has been analyzed theoretically and checked experimentally by Bromley (ref. 1). His analysis gave the following expression for the heat-transfer coefficient:

$$\frac{hD^{1/4}}{F_o} = 0.62 \tag{1}$$

where F_o is the property group

$$F_o = \left[\frac{k^3 \rho(\rho_l - \rho) g \lambda_1^*}{\mu \Delta T}\right]^{1/4} \tag{2}$$

and λ^* is the modified latent heat of vaporization

$$\lambda_1^* = \lambda \left(1 + \frac{0.4\ C_p\ \Delta T}{\lambda}\right) \tag{3}$$

(All symbols are defined in appendix A.) To model the phenomenon, Bromley assumed that the generated vapor flowed laminarly in a thin vapor annulus surrounding the heated cylinder. This model fit the experimental data for a range in diameters from 1/4 to 1 inch (0.635 to 1.91 cm), for many common fluids.

In 1953, Banchero, et al., (ref. 2) furthered the understanding of film boiling. Using liquid oxygen as a primary test fluid, they assessed the effects of wire size and pressure on the film-boiling process. They pointed out that Bromley's equation is valid over a narrow range of wire sizes and recommended an empirical modification:

$$h = a\left(\frac{1}{D} + C\right) F_o \tag{4}$$

Here a is nearly constant and C is a constant for each fluid tested, D is the diameter, and F_o is the property group of Bromley's equation.

In 1961, Berenson (ref. 3) used a critical wavelength parameter,

$$\lambda_c = 2\pi \sqrt{\frac{\sigma g_c}{(\rho_l - \rho) g}}$$

to correlate film boiling from a horizontal surface:

$$\frac{h \lambda_c^{1/4}}{F_o} = 0.672 \tag{5}$$

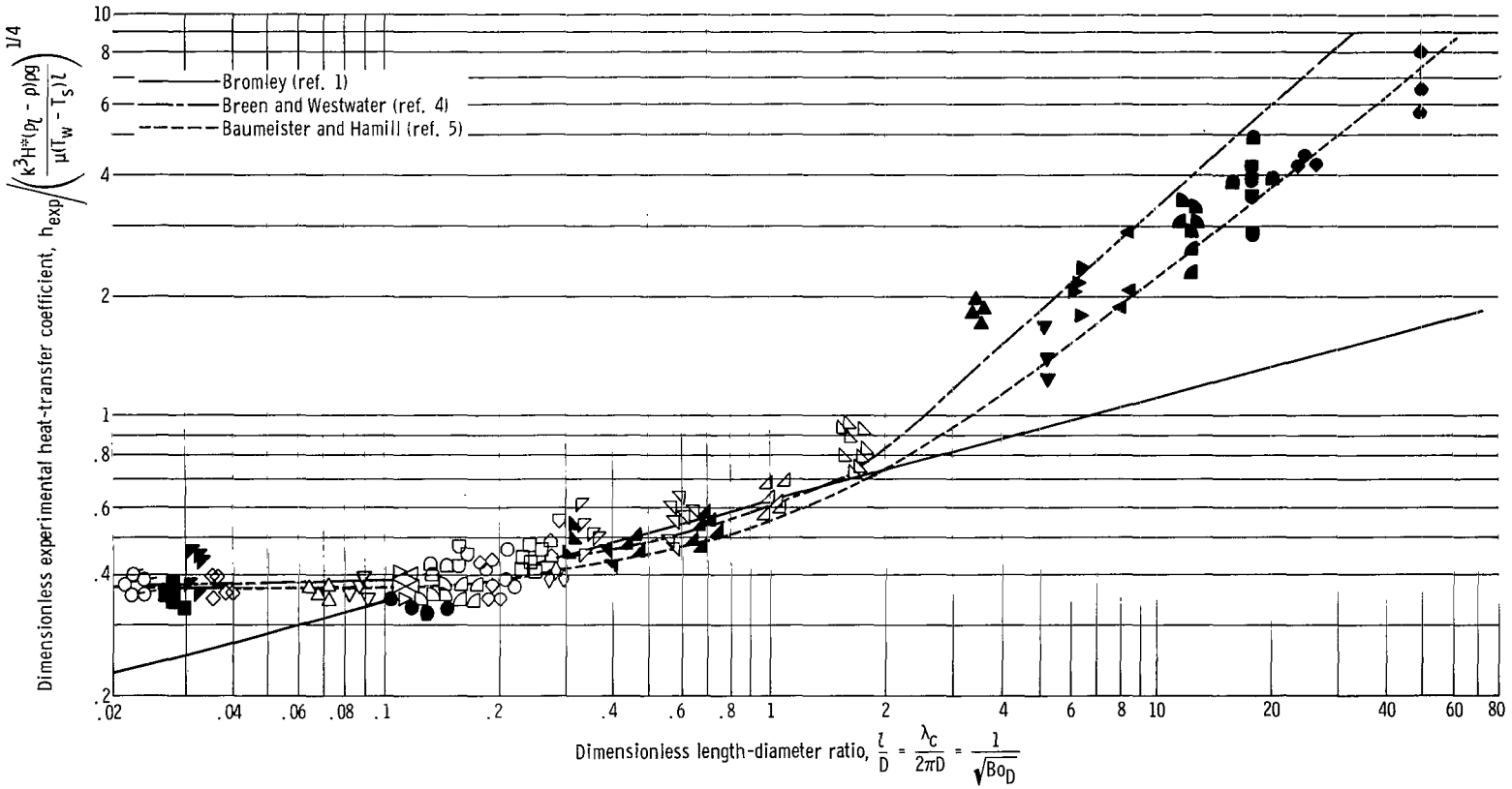

Figure 1. - Heat-transfer coefficient in film boiling from horizontal cylinders as function of characteristic diameter ratio. Data from Breen and Westwater (ref. 4). Each type of data point represents a set of test conditions within the following ranges: Fluids, water, helium, oxygen, pentane, nitrogen, ethanol, benzene, Freon-113, isopropanol, or carbon tetrachloride; temperature, 72° to 2600° F (301 to 1703 K); heat-transfer rate, 17 to 2120 Btu per hour per square foot per °F (97 to 12 200 W/(m^2)(K)); cylinder diameter, 0.00053 to 4.6 centimeters; critical wavelength, 0.068 to 0.660 inch (0.173 to 1.67 cm); length-diameter ratio, 0.135 to 50.

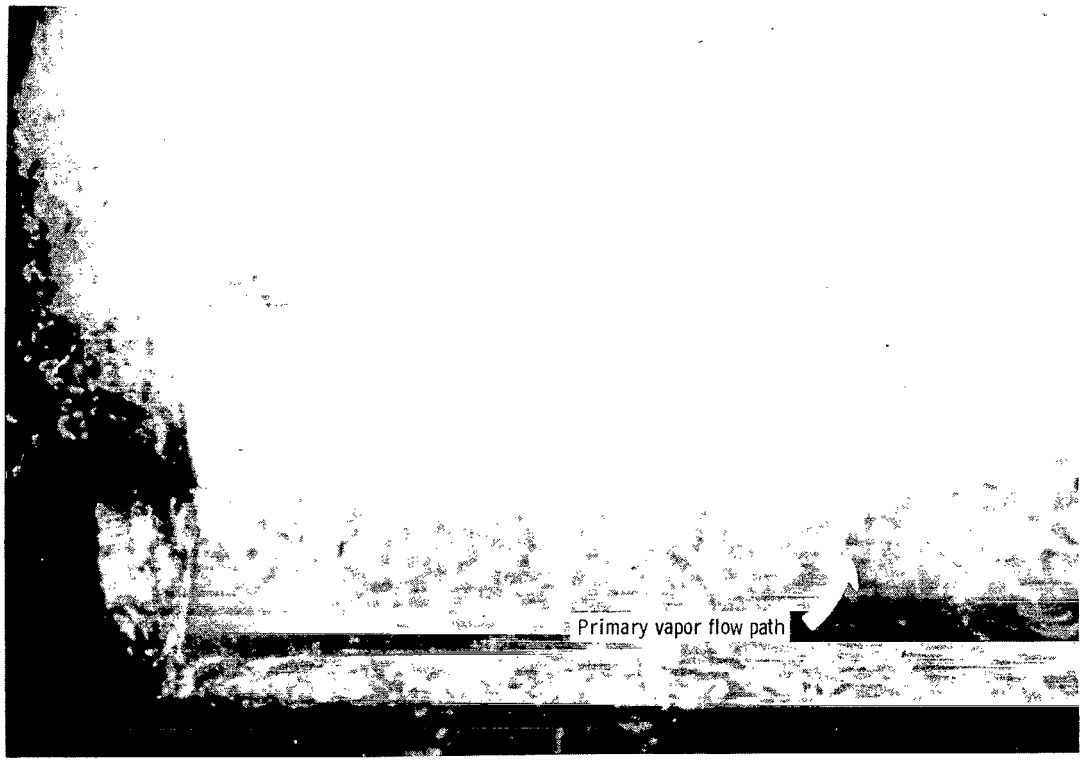

(a) Fluid, liquid nitrogen; wire diameter, 1.75 inches (4.76 cm); ratio of critical wavelength to diameter, 0.1435.

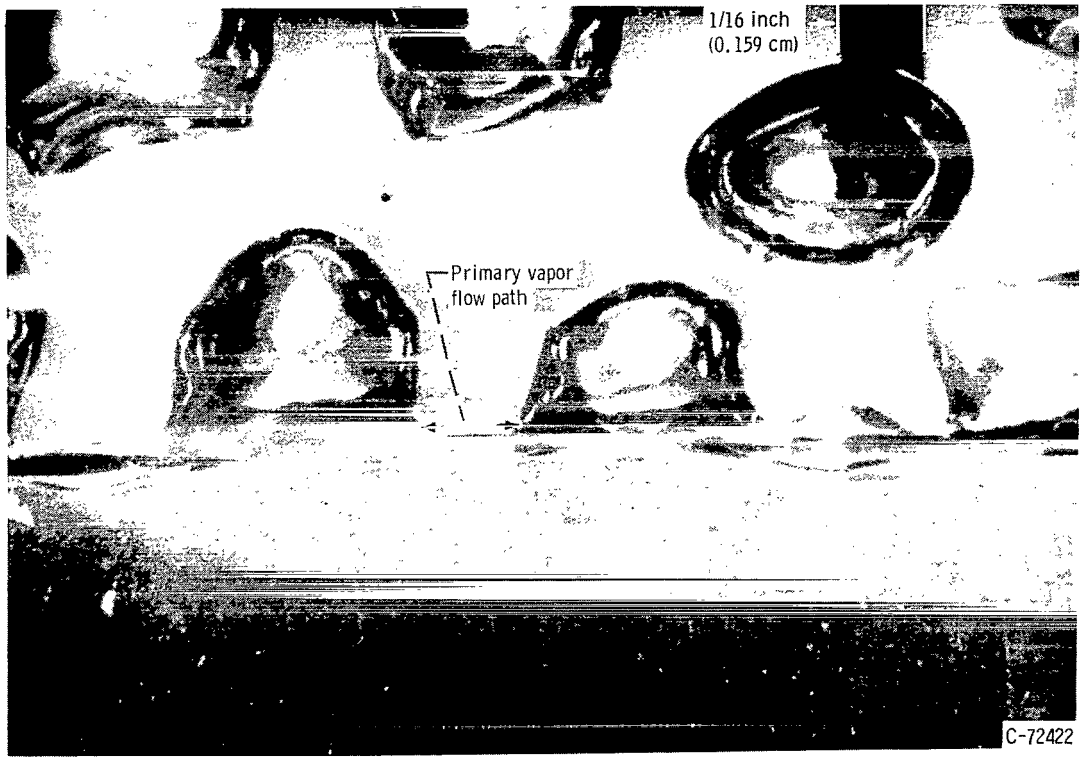

(b) Fluid, ethyl alcohol; wire diameter, 0.02 inch (0.0507 cm); ratio of critical wavelength to diameter, 20.

Figure 2. - Effect of diameter on film boiling from horizontal wires.

A year later, in 1962, Breen and Westwater (ref. 4) made another significant contribution to the understanding of film boiling. Introducing the critical wavelength λ_c, they correlated all available film-boiling heat-transfer data for horizontal cylinders by means of a simple empirical equation. The correlation is illustrated in figure 1. This again demonstrates the Bromley equation to be valid over a narrow range of wire sizes.

Baumeister and Hamill (ref. 5) developed a theoretical model for film boiling from small-diameter wires which followed the trend in the experimental data and gave excellent agreement with the Breen and Westwater correlation.

As seen in figure 1, below an ℓ/D of 0.1 the heat-transfer data are independent of wire size, whereas Bromley's equation predicts ever decreasing values of the heat-transfer coefficient. The heat-transfer coefficient in this regime was correlated by Breen and Westwater (ref. 4) using Berenson's results (ref. 3) for film boiling off an upward-facing flat plate. This correlation appears as a horizontal line in figure 1.

Above an ℓ/D of 2, the heat-transfer data rise at a much quicker rate than the Bromley equation would predict. The increase in the data slope for small wires (large ℓ/D) results primarily from a change in the flow profiles around the wire, as displayed in the photographs in figure 2. For large-diameter wires (fig. 2(a)), the flow is circumferential and pseudoturbulent in nature. The flow follows a vertical pattern upward and leaves the wire in a large dispersed vapor column. However, for small-diameter wires, as shown in figure 2(b), the flow is axial into vapor domes that are periodically distributed along the wire. These domes grow as additional vapor enters, eventually break away from the wire, and escape as large vapor bubbles into the bulk liquid. The upper photographs of figure 3 illustrate how the vapor patterns change with ℓ/D for cylinders ranging from 0.0508 to 4.76 centimeters in diameter. Note the changes in vapor structure and wave patterns near the transition regime.

Frederking, et al., (refs. 6 and 7) performed an analysis similar to Bromley's (ref. 1) for relatively large-diameter spheres. The results of this analysis did not fit their data. They then suggested an empirical correlation based upon the parameters of turbulent free convection with the property group to the 1/3 power, which fit most of their data.

Photographs of film boiling from spheres in liquid nitrogen show a phenomenon similar to that observed on wires of corresponding diameter (see fig. 3). Here, the small-diameter wires and spheres (large ℓ/D) both exhibit the characteristic vapor dome. As evidenced by the series of domes rising from the small-diameter spheres, the process of vapor removal is periodic in nature. Motion pictures of the phenomenon (see appendix H and film supplement) indicate that the flow around the spheres which supplies the growing vapor domes is laminar in nature with small capillary waves moving upward along the liquid-vapor interface. For large-diameter wires and spheres, however, the

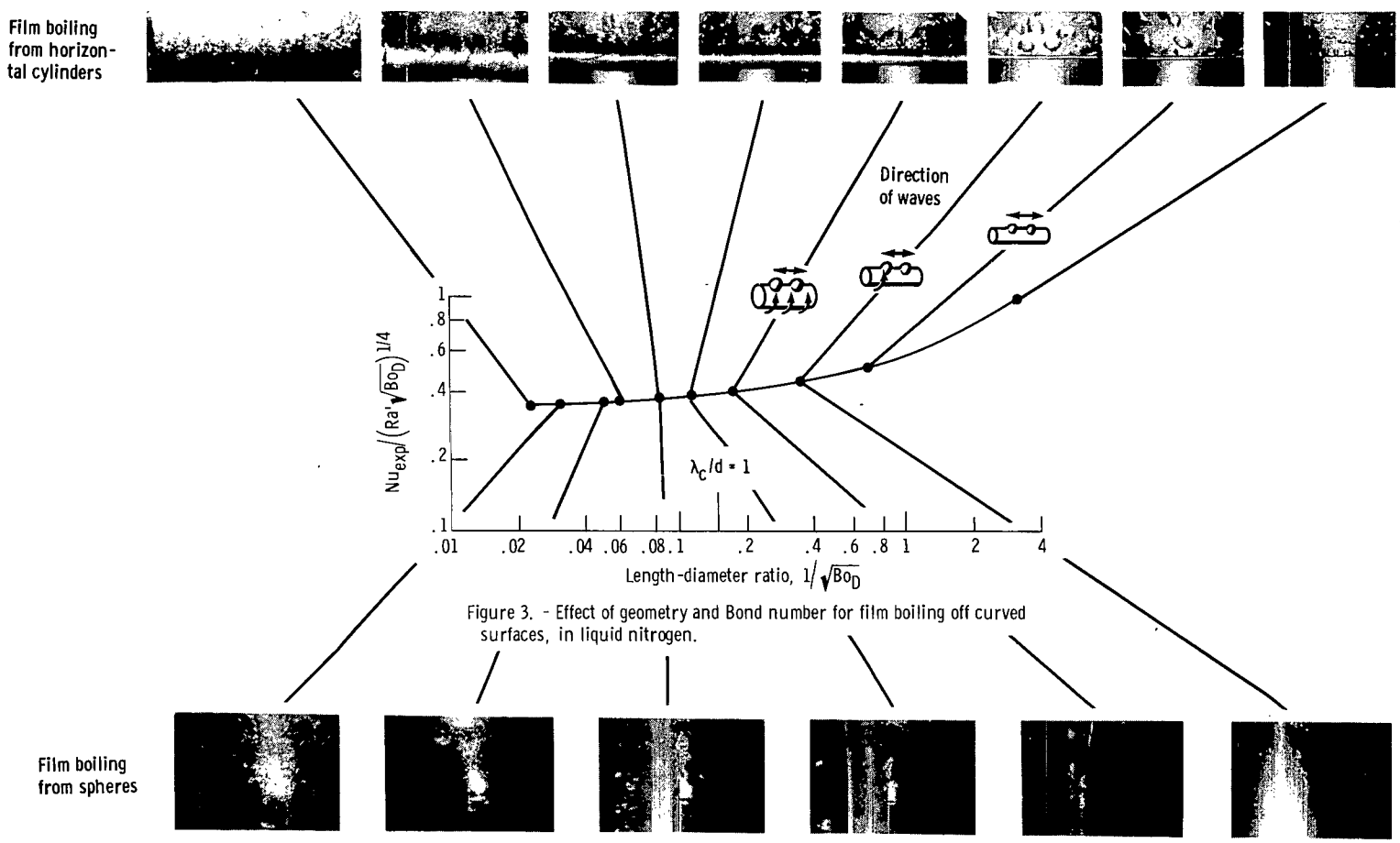

Figure 3. - Effect of geometry and Bond number for film boiling off curved surfaces, in liquid nitrogen.

flow appears turbulent and chaotic in nature at all positions surrounding both the wire and the sphere, except near the lower stagnation region. Because of this strong evidence for similarity between boiling on a wire and a sphere, we felt that the theoretical techniques used to analyze the wire could be applied to film boiling off spheres.

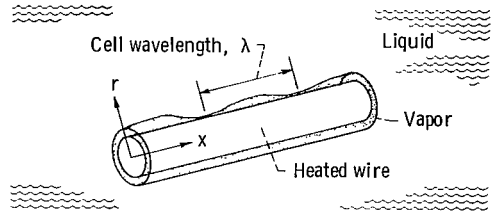

(a) Small-diameter wires ($\ell/D > 2$), reference 5.

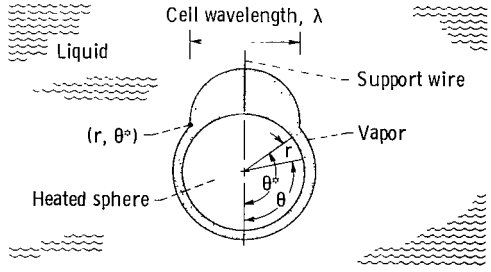

(b) Small-diameter spheres.

Figure 4. - Film-boiling models for small-diameter wires and spheres.

The theoretical model for small-diameter wires (ref. 5) was a modification of Berenson's original model introduced for film boiling from flat surfaces. A schematic of the model is shown in figure 4(a). A further modification of the vapor dome model to the case of film boiling from small-diameter spheres is depicted in figure 4(b). Here, the vapor is generated in the thin annular region at the bottom of the sphere. It then flows in a laminar manner into the escape dome. In the physical situation, the vapor domes grow as additional vapor enters, eventually breaking away from the sphere and escaping as large vapor bubbles into the bulk liquid. The proposed model, to be discussed in detail in the next section, assumes the existence of a time-average configuration where all the velocity, pressure, and temperature fields are at steady state.

Heat-transfer expressions for both large- and small-diameter spheres are developed herein. The data are shown to be bounded by the slip and nonslip boundary conditions; however, the shifts from one condition to another are unexplainable without further analysis. For small spheres, a theoretical expression based on the model depicted in figure 4(b) is derived and compared with the available film-boiling data. For large-diameter spheres, the film-boiling heat-transfer coefficient is correlated by matching the small-sphere and flat-plate solutions; a similar technique is used for film boiling off of a large cylinder. In this case, the heat-transfer coefficient is independent of geometry and depends only on a fluid property group raised to the 1/4 power.

In addition, a motion-picture study of film boiling was undertaken to assess the nature of the vapor flow from spheres, cylinders, and a vertical flat plate. A motion-picture supplement C-263 has been prepared and is available on loan. A request card and a description of the film are included at the back of this report.

BASIC MODEL AND EQUATIONS

Consider the single-dome model of a submerged sphere in film boiling, as illustrated in figure 5. The physical situation could be a solid metal sphere supported on a wire

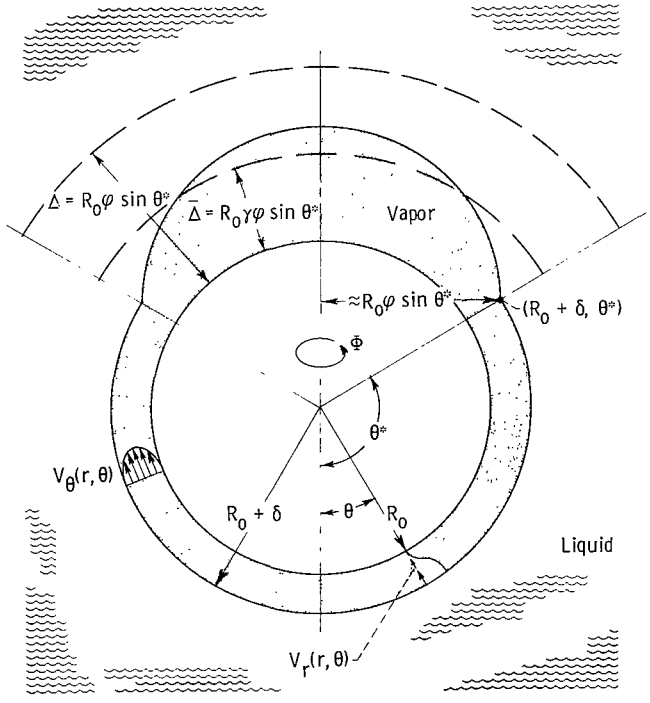

Figure 5. - Schematic model of film boiling off submerged sphere, single-dome case.

and immersed in liquid nitrogen - provided, of course, that the proper temperature difference is maintained. The material evaporated at the interface flows about the sphere towards the vapor reservoir. The reservoir begins at the point designated as $(R_o + \delta, \theta^*)$ in figure 5.

The single-dome model appears to represent film boiling from small spheres (low Bond number, Bo) as shown in figure 3. However, for large-diameter spheres (large Bond numbers) the single dome appears to give way to multiple domes, such as occur off a horizontal plate facing upward. Apparently, as with boiling off horizontal wires, as the size of the sphere becomes larger than the critical wavelength λ_c, from hydrodynamic stability theory $\left(\lambda_c = 2\pi D/\sqrt{Bo_D}\right)$, the single dome tends towards multiple domes. To maintain a tractable solution for the large-sphere case, the conduction area under the single dome is assumed to be replaced by multiple-dome film boiling. This multiple-dome film-boiling regime, for large spheres, is assumed to be similar to film boiling from an upward-facing flat plate.

There are, of course, several possible modes of heat transfer as the sphere temperature tends toward the Leidenfrost temperature (ref. 8). These mechanisms (nucleate boiling, etc.) are beyond the scope of our investigation; hence, our model is restricted to the developed film-boiling regime.

The following assumptions are made in developing the single- or multiple-dome models:

(1) Rotational and vibration effects due to the sphere are small.

(2) Surface capillary waves, while influencing the boundary, do not significantly alter the heat transfer or the laminar nature of the flow.

(3) The vapor gap thickness is constant.

(4) The model has complete symmetry with respect to the Φ coordinate.

(5) Because of the low Reynolds number, the flow of vapor is laminar and incompressible; and the inertia and body force terms in the Navier-Stokes equations, as applied to the vapor, are neglected. Justification for this assumption can be found in reference 9.

(6) Radiation is negligible.

(7) The velocity and temperature profiles are in steady state.

(8) At any instant of time, the sphere is at an average temperature $\overline{T}_w$, and the evaporating liquid is at the saturation temperature T_s. The properties of the flow field are evaluated at the film temperature

$$T_f = \frac{\overline{T}_w + T_s}{2}$$

and are constant (an assumption that has worked quite well, ref. 10).

(9) The convective terms in the energy equation are neglected; however, the latent heat of vaporization is corrected to accommodate this assumption. The correction is usually of the form

$$\lambda^* = \lambda \left[1 + \frac{1}{2}\left(C_p \frac{\Delta T}{\lambda}\right)\right] \tag{6}$$

Such assumptions are apparently valid, based on the work in references 8 to 11. These authors indicate the major mode of heat transport to be conduction; when the convection term is retained, the solution yields a factor analogous to the effective latent heat of vaporization λ^*. Thus, it is assumed that, in the energy equation,

$$\frac{V_\theta}{r}\frac{\partial T}{\partial \theta} < V_r \frac{\partial T}{\partial r} << \frac{\kappa}{r^2}\frac{\partial}{\partial r}\left(r^2 \frac{\partial T}{\partial r}\right) \tag{7}$$

$$\frac{1}{r^2 \sin\theta}\frac{\partial}{\partial \theta}\left(\sin\theta \frac{\partial T}{\partial \theta}\right) < \frac{1}{r^2}\frac{\partial}{\partial r}\left(r^2 \frac{\partial T}{\partial r}\right) \tag{8}$$

The surrounding liquid is at the saturation temperature. Thus, all the heat reaching the liquid produces vapor.

The governing equations are as follows (ref. 12):

(1) Momentum:

$$0 = -\frac{g_c}{\rho}\frac{\partial P}{\partial r} + \nu\left(\nabla^2 V_r - \frac{2V_r}{r^2} - \frac{2}{r^2}\frac{\partial V_\theta}{\partial \theta} - \frac{2}{r^2} V_\theta \cot\theta\right) \tag{9}$$

$$0 = -\frac{g_c}{\rho}\frac{1}{r}\frac{\partial P}{\partial \theta} + \nu\left(\nabla^2 V_\theta + \frac{2}{r^2}\frac{\partial V_r}{\partial \theta} - \frac{V_\theta}{r^2 \sin^2\theta}\right) \tag{10}$$

where

$$\nabla^2 = \frac{1}{r^2}\frac{\partial}{\partial r}\left(r^2 \frac{\partial}{\partial r}\right) + \frac{1}{r^2 \sin\theta}\frac{\partial}{\partial \theta}\left(\sin\theta \frac{\partial}{\partial \theta}\right) \tag{11}$$

(2) Energy:

$$0 = \frac{\partial}{\partial r}\left(r^2 \frac{\partial T}{\partial r}\right) \tag{12}$$

(3) Continuity:

$$0 = \frac{1}{r^2}\frac{\partial}{\partial r}(r^2 V_r) + \frac{1}{r \sin\theta}\frac{\partial}{\partial \theta}(V_\theta \sin\theta) \tag{13}$$

The boundary conditions are separated into two categories, which represent the single-vapor-dome and multiple-vapor-dome regimes, respectively.

Regime	Surface	Single-dome model	Multiple-dome model	Equation number
Thin film	$r = R_o$	$V_r = 0,\ V_\theta = 0,\ T = \overline{T}_w$		(14)
	$r = R_o + \delta$ $\theta < \theta^*$	$V_r = V_r(\delta),\ V_\theta = 0,\ T = T_s$		(15)
	$\theta = 0$ $R_o \le r \le R_o + \delta$	$V_\theta = 0$		(16)
	$\theta = \theta^*$ $r = R_o + \delta$	$P = P_d$		(17)
Vapor dome	$\theta^* \le \theta < \pi$	Heat transfer by conduction	$\frac{hD}{k} \propto \left(Ra' \sqrt{Bo_D}\right)^{1/4}$	(18)

where θ^* is defined (fig. 4) as the transition from the thin film to the vapor dome, δ is the vapor gap thickness, and P_d is the dome pressure.

The boundary conditions are incomplete at this point since δ, θ^*, and $V_r(\delta)$ are unknowns. Hence, three additional mathematical constraints are necessary to make the problem tractable.

(4) Static pressure balance:

One additional constraint requires the sphere to be in static equilibrium. Small vibrations of the sphere are neglected. The static equilibrium condition requires that the average pressure $\overline{P}$ in the vapor at the liquid-vapor interface resulting from the

weight of the supported liquid, surface tension, and atmospheric pressure balance the average pressure due to flow (see appendix C). Summing the forces acting at the interface gives

$$\int_0^{2\pi} \int_0^{\theta^*} P\Big|_{R_o+\delta} (R_o + \delta)^2 \sin\theta \, d\theta \, d\Phi = \int_0^{2\pi} \int_0^{\theta^*} \overline{P}(R_o + \delta)^2 \sin\theta \, d\theta \, d\Phi \quad (19)$$

The total pressure in the vapor gap P can be calculated from the momentum equations, and $\overline{P}$ is established in appendix B, along with a solution to the momentum equations.

(5) Interface energy balance:

The second additional constraint is the interface energy balance. Because the supporting fluid is assumed to be at the saturation temperature (assumption 8), all the heat reaching the interface produces evaporation of the fluid material. Mathematically, this constraint is expressed as

$$-\rho\lambda V_r(R_o + \delta, \theta) = -k \frac{\partial T}{\partial r}\Big|_{r=R_o+\delta} \quad (20)$$

where λ is the latent heat of vaporization and

$$-k \frac{dT}{dr}\Big|_{r=R_o+\delta}$$

is the conduction heat flux of the boundary of the surrounding liquid.

(6) Entropy production:

The third constraint is that the rate of entropy production be a maximum. As θ^* is the parameter which controls the rate of exchange of energy (maximization of entropy production),

$$\frac{\partial h}{\partial \theta^*} = 0$$

$$\frac{\partial^2 h}{\partial \theta^{*2}} < 0 \quad (21)$$

Equation (21) will lead to the determination of θ^* as a function of Bond number Bo. For a constant area, h represents the rate of exchange of energy per degree change in temperature, which in a loose thermodynamic sence, "quasi-equilibrium," describes entropy production.

This optimization technique has been used successfully in predicting the heat-transfer rates in film boiling from flat plates (ref. 13) and wires (refs. 5 and 14).

(7) Slip and nonslip boundary condition:

The analysis herein depends on the nonslip boundary condition, $V_\theta\Big|_{\zeta=\varphi} = 0$, equation (15). However, the analysis using an apparent or virtual slip boundary condition

$$\frac{\partial V_\theta}{\partial \zeta}\Bigg|_{\zeta=\varphi} = 0 \tag{22}$$

is carried out in appendix F. In subsequent material unless otherwise specified, the nonslip analysis is used.

ANALYTICAL RESULTS

The governing equations, along with the appropriate boundary conditions and constraints, are solved in appendixes B, C, D, and E. Only the results are presented in the main text.

Normally, the experimental data represent an average of more than one mode of heat transfer from the sphere. Thus, the theoretical heat-transfer coefficient is formulated as the sum of the two major modes of heat transport, film boiling and conduction through the vapor dome. With this formulation, theory and data can be compared. For a given fluid, the terms small Bond number and small sphere are used interchangeably, although the precise meaning of each is distinct.

Small-Bond-Number Case

For a small-diameter sphere, such as shown in the lower far right photograph of figure 3, the model shown in figure 5 applies. The heat-transfer coefficient may be written as

$$h_{small} = h_1 \frac{A_1}{A_t} + h_2 \frac{A_2}{A_t} \tag{23}$$

$$= \begin{matrix} \text{Film-boiling} \\ \text{(transport across} \\ \text{thin vapor film} \\ (\theta < \theta^*)) \end{matrix} + \begin{matrix} \text{Conduction} \\ \text{(transport through} \\ \text{vapor dome)} \end{matrix}$$

where A_1 is the lower surface area of the sphere ($\theta < \theta^*$), and h_1 is the associated film-boiling heat-transfer coefficient for this area. In the second term, A_2 represents the surface area beneath the dome, and h_2 represents the conduction heat-transfer coefficient associated with this area.

In order to compare theoretical and experimental results, h_{small} represents an area-weighted average heat-transfer coefficient from the sphere. Here, A_t represents the total surface area of the sphere, the sum of A_1 and A_2.

The solution for h_{small} is given by equation (B65) of appendix B as

$$Nu' = 1/4 \left[\frac{-2Ra'G(Bo)}{3}\right]^{1/4} + \gamma^{-1}(1 + \cos\theta^*)\csc\theta^* \tag{24}$$

where

$$Nu' = 2\left(\frac{hR_o}{k} - 1\right) \tag{25}$$

$$Ra' = \frac{\rho(\rho_l - \rho)gD^3\lambda^*}{k\mu\Delta T} \tag{26}$$

and Nu' and Ra' are modified Nusselt and Rayleigh numbers, respectively. The function G(Bo) (fig. 6(a)) depends on the Bond number,

$$Bo = \frac{(\rho_l - \rho)gR_o^2}{\sigma g_c} = \frac{\text{Buoyancy forces}}{\text{Surface-tension forces}} \tag{27}$$

For a fluid at its normal boiling point, Bond number varies, essentially, as the square of sphere radius (i. e., as the size of the sphere). Other conditions, such as approaching the critical point or large variations in g, would effect a variation in Bond number for a fixed radius.

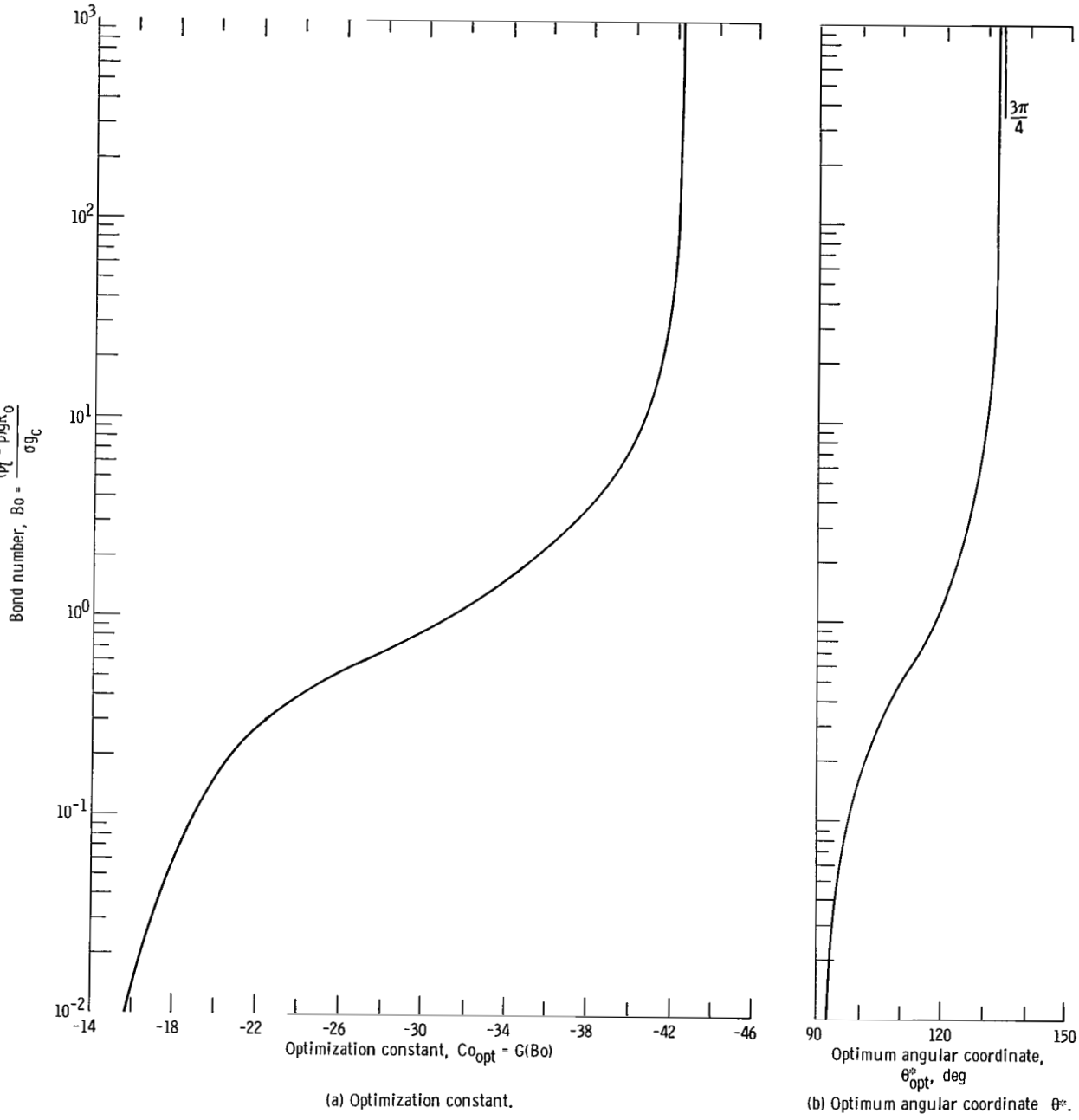

(a) Optimization constant.

(b) Optimum angular coordinate θ^*.

Figure 6. - Locus of optimization constant Co_{opt} and optimum angular coordinate θ^* as function of Bond number.

In addition, the angle θ^* in equations (15), (17), and (18) is a function of Bond number. The functional relation is shown in figure 6(b). As shown in this figure, the analysis predicts an upper bound in the value of θ^* to be $3\pi/4$, as illustrated in figure 6(b). The limit appears to agree with physical observations on boiling from small spheres (see fig. 3); however, it is also apparent from the other spheres of figure 3 that the magnitude of Bo is quite a significant factor.

Bond Number Range for Small-Sphere Model

Considering the expression for the heat-transfer coefficient for small spheres, there remains one intriguing question. Over what range of Bond numbers can this analysis be applied? As the Bond number increases, experiments have demonstrated that a single dome no longer appears, rather multiple domes appear (lower photographs, fig. 3).

From hydrodynamic stability theory, the most dangerous wavelength λ_{md} is defined as

$$\lambda_{md} = \sqrt{3}\,\lambda_c = \sqrt{3}\left(\frac{(\rho_l - \rho)g}{\sigma g_c}\right)^{1/2} \tag{28}$$

For the case of a heavy liquid over a lighter fluid, the most dangerous wavelength represents the wavelength of a small sinusodial unstable disturbance, which has the fastest amplitude growth rate of all possible unstable disturbances. For the purpose of this analysis, it is assumed that if the circumference is less than the most dangerous wavelength, that is, if

$$R_o\theta^* \leq \lambda_{md} \tag{29}$$

the model and heat-transfer equation (24) would apply. Noting that

$$\frac{R_o}{\lambda_c} = \frac{\sqrt{Bo}}{2\pi} \tag{30}$$

it follows that for

$$Bo^* \leq \left(\frac{2\pi\sqrt{3}}{\theta_{max}}\right)^2 \tag{31}$$

the analysis is valid. (θ_{max} can be found from fig. 6(b).) This Bond number Bo* predicts with reasonable accuracy the transition from single-dome film boiling to multiple-dome film boiling, as shown in figure 3. Consequently, to determine the heat transfer for Bo > Bo*, the analytic model must be modified.

Large-Bond-Number (Large Sphere) Modification

When the Bond number is greater than that given by equation (31), multiple domes replace the single domes (see figs. 7 and 3). Of course, for these larger Bond numbers,

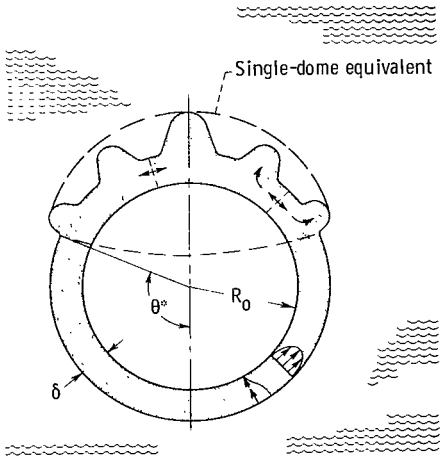

Figure 7. - Film boiling off submerged large sphere, multiple-dome case.

the expression for the heat-transfer coefficient given by equation (24) would no longer apply.

Since, at the present time, all available experimental data exist for Bond numbers near and outside the range of equation (24), the small-sphere analysis cannot be readily compared with data. It is desirable for practical use, however, to modify the theoretical analysis so that data can be correlated over a more complete spectrum of Bond numbers.

The solution determined to within a constant α is found in appendix E. The solution for the large-Bond-number case (large spheres) becomes

$$\frac{Nu'}{\left(Ra' \sqrt{Bo}\right)^{1/4}} = \frac{1}{4}\left[\frac{-2G(Bo)}{3\sqrt{Bo}}\right]^{1/4} + 0.21(1 + \cos \theta^*) \tag{32}$$

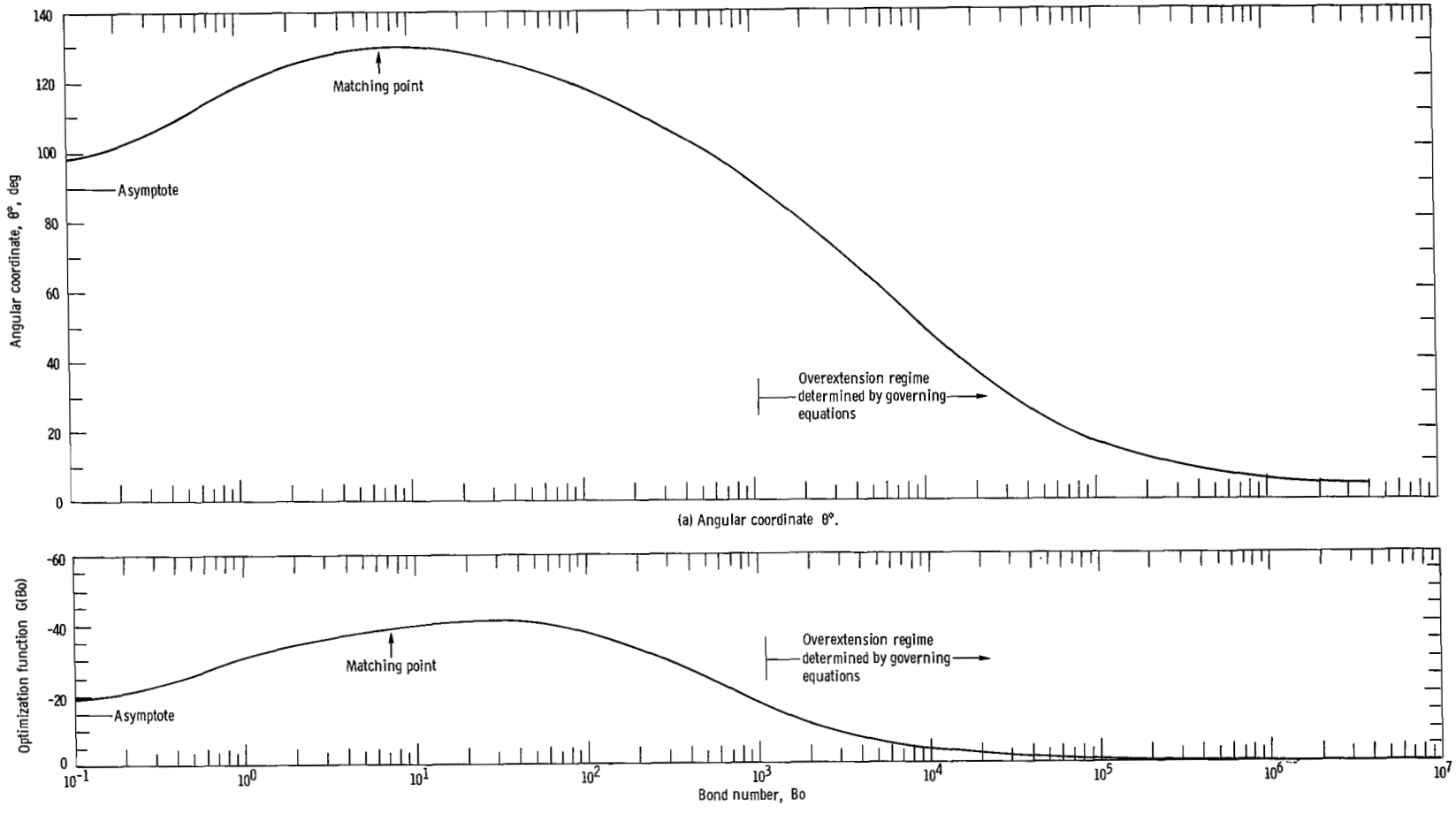

(a) Angular coordinate θ*.

(b) Optimization function G(Bo).

Figure 8. - Angular coordinate θ* and optimization function G(Bo) as function of Bond number.

General Solution

The solutions to the large- and small-Bond-number regimes (large and small spheres) in essence represent two asymptotic cases. In appendix E, the two solutions are matched at $R_0\theta^*/\lambda_c = 1$, and a linear combination of the two solutions produces a general solution applicable to both the small- and the large-Bond-number regimes

$$\frac{Nu}{\left(Ra'\sqrt{Bo_D}\right)^{1/4}} = \frac{1}{4}\left[\frac{-2G(Bo)}{3\sqrt{Bo_D}}\right]^{1/4} + \left[0.177 + \frac{\csc\theta^*}{\left(Ra'\sqrt{Bo_D}\right)^{1/4}}\right](1 + \cos\theta^*) \tag{33}$$

where Bo_D is Bond number based on sphere diameter to facilitate comparison to data.

The functions $G(Bo)$ and θ^* are extended to the large Bo regime and plotted in figures 8(a) and (b).

As shown in equation (33), if $Bo_D \ll 1$, the first term dominates, and the expression for the Nusselt number reduces to equation (24), the expression for the heat-transfer coefficient for small spheres. For large Bond numbers, equation (33) approaches

$$Nu' = 0.177\left(Ra'\sqrt{Bo_D}\right)^{1/4}(1 + \cos\theta^*) + \frac{1}{4}\left[\frac{-2G(Bo)Ra'}{3}\right]^{1/4} \tag{34}$$

The first term of this expression is the classical expression of film boiling from a flat plate facing upward times an area correction factor, while the second term represents film boiling from the lower portion of the sphere.

The constant coefficients of equation (34) depend not only on the physical process but also on the boundary conditions. The slip and nonslip conditions are the most commonly considered variation in boundary conditions for this type of problem and are discussed in the next section.

Slip Modification

In the analysis presented in appendix F, it is assumed that the nonslip boundary condition $V_\theta\Big|_{\zeta=\varphi} = 0$ (eq. (15)) occurs at the liquid-vapor interface. Bromley (ref. 1), however, showed that the slip boundary condition, along with the nonslip boundary condition, bracketed the experimental data. For this particular problem, the slip boundary condition (eq. (15)) becomes

$$\left.\frac{\partial v_\theta}{\partial \zeta}\right|_{\zeta=\varphi} = 0 \tag{22}$$

The details of the modification are given in appendix F. The results of this modification are as follows:

(1) Small-diameter sphere: Equation (24) becomes

$$Nu' = \sqrt{2}\left\{\frac{1}{4}\left[\frac{-2Ra'G(Bo)}{3}\right]^{1/4} + \gamma^{-1}(1 + \cos\theta^*)\csc\theta^*\right\} \tag{35}$$

(2) Large-diameter sphere: Equation (32) becomes

$$\frac{Nu'}{\left(Ra'\sqrt{Bo}\right)^{1/4}} = \sqrt{2}\left\{\frac{1}{4}\left[\frac{-2G(Bo)}{3\sqrt{Bo}}\right]^{1/4} + 0.21(1 + \cos\theta^*)\right\} \tag{36}$$

(3) Combined solution: Equation (33) becomes

$$\frac{Nu'}{\left(Ra'\sqrt{Bo_D}\right)^{1/4}} = \sqrt{2}\left\{\frac{1}{4}\left[\frac{-2G(Bo)}{3\sqrt{Bo_D}}\right]^{1/4} + \left[0.177 + \frac{\csc\theta^*}{\left(Ra'\sqrt{Bo_D}\right)^{1/4}}\right](1 + \cos\theta^*)\right\} \tag{37}$$

In the next section, the results for both the slip and nonslip cases (refs. 7, 15, and 16) are compared with available experimental data.

DISCUSSION

In reference 7, a transient cooldown technique was used to determine the film-boiling heat-transfer coefficient. The data were obtained from two spheres submerged in two fluids. The sphere diameters were 1/4 and 3/8 inch (0.635 and 0.95 cm) and the fluids were nitrogen and helium. The results of these tests are replotted in figure 9 in terms of Nusselt number Nu and modified Rayleigh number Ra'. The helium data and the nitrogen data for the 1/4-inch (0.635-cm-) diameter sphere follow the 1/4-power rule; however, note that the helium data are near the theoretical "slip" line given by equation (35), while the nitrogen data (1/4-in. - (0.635-cm-) diam sphere) are near the theoretical line given by equation (24). Note that the nitrogen data for the 3/8-inch-(0.95-cm-) diameter sphere tend to follow a 1/3-power rule, on the average.

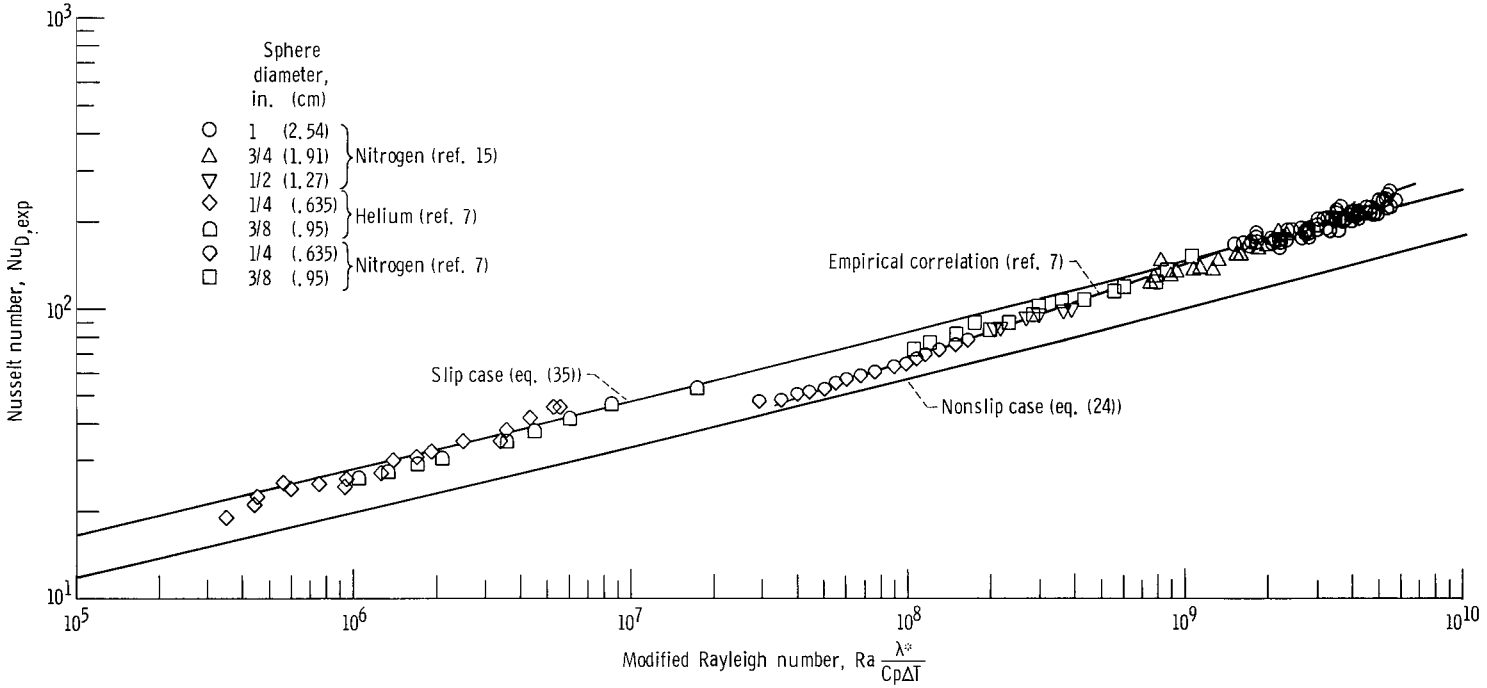

Figure 9. - Transient film boiling off spheres. Results from references 7 and 8.

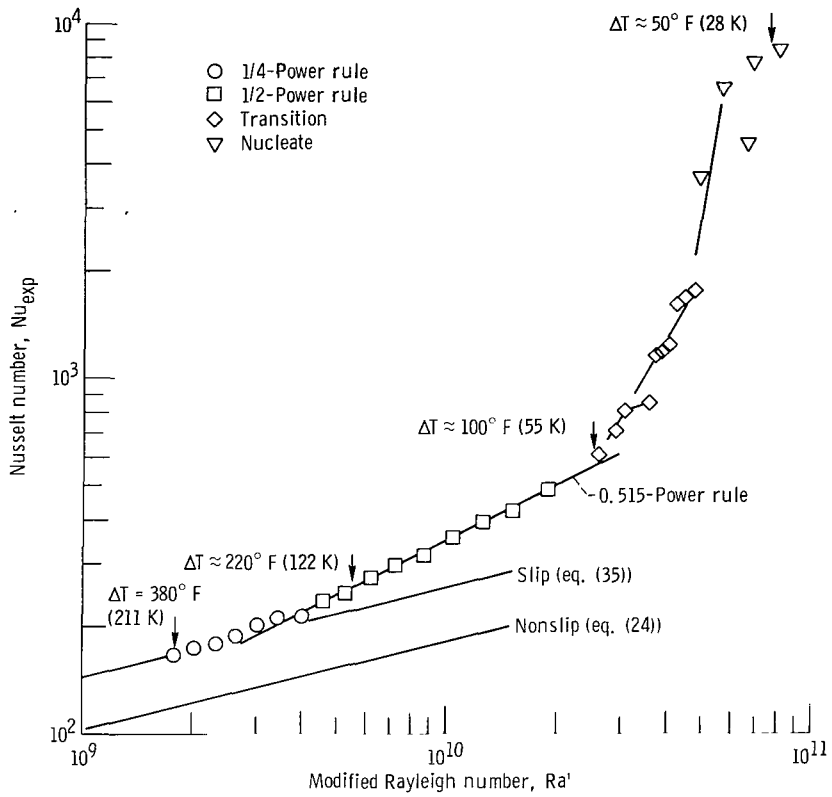

Figure 10. - Variation in Nusselt number with modified Rayleigh number for transient cooldown of 1-inch- (2.54-cm-) diameter sphere in liquid nitrogen (ref. 8).

More recently, transient cooldown data were obtained in reference 8 for liquid nitrogen with 1/2-, 3/4-, and 1-inch- (1.27-, 1.90-, and 2.54-cm-) diameter submerged spheres. These data indicate that several power rules may apply, depending on the mode of heat transfer. This is illustrated for the 1-inch- (2.54-cm-) diameter sphere in figure 10. The circular symbols appear to follow the theoretical "slip" line (eq. (35)). However, much of the data tend to follow a 0.515 or square-root power rule, followed by the usual large increase in heat transfer at nucleate boiling. In a private communication, Lyle Gordon Rhea indicated that the shift to the 0.515-power rule was a result of nucleate boiling on the stem which supported the sphere.

With these limitations in mind (cf. large temperature differences and film boiling only) the data of reference 2 were replotted in figure 11 along with data from figure 10. These data represent temperature differences greater than 210° F (~117 K) and no change to the square-root rule. These data follow the 1/4-power rule; however, they tend to shift between the slip and nonslip theoretical lines predicted by equations (35) and (24), indicating a change in the model.

Results similar to those reported in references 7 and 15 were obtained earlier in reference 16 (analyzed in ref. 6) for a 1-inch- (2.54-cm-) diameter sphere submerged

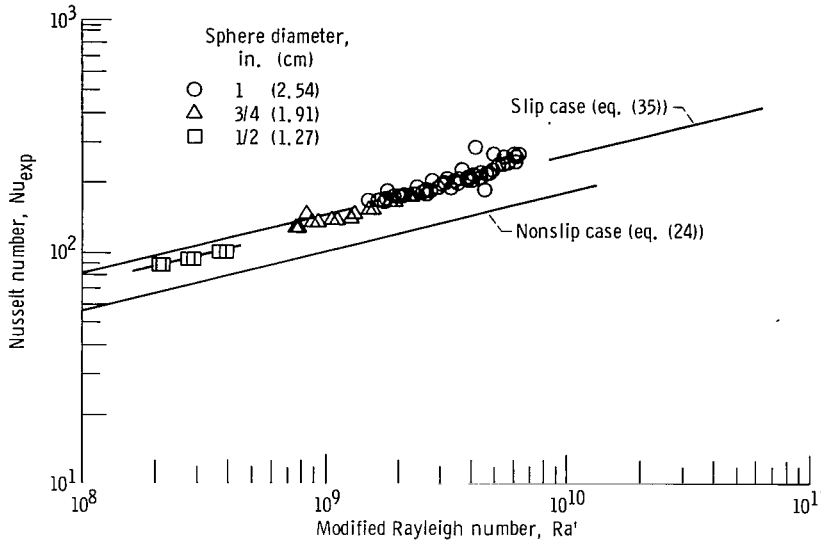

Figure 11. - Transient film-boiling data for 1/2-, 3/4-, and 1-inch- (1.27-, 1.91-, and 2.54-cm-) diameter spheres submerged in liquid nitrogen. Selected data from reference 15; temperature difference between heater wall and saturation, >210° R and prior to ← in the data of reference 15.

in liquid nitrogen. From the results of that analysis, it would appear that the data again follow the 1/3-power rule; however, these data might also follow the 1/4-power rule if similar temperature limitations were applied.

The data of figure 9 appear to be bounded by the slip and nonslip equations (eqs. (35) and (24)). Would these data be bounded for larger or smaller spheres? And what is the mechanism which causes the transition from one curve to the other? The answers to these questions appear to be based on geometry and fluid properties, which suggests that some critical dome size is involved. As indicated earlier, the Bond number equation (eq. (27)) constitutes a parameter which incorporates these effects.

Bond number is a natural parameter of this analysis and has been successfully applied to film boiling from a wire (ref. 5); it is also natural to assume that film boiling from a sphere should show similar trends. The photographs of reference 7 and this report seem to agree with such a classification. The critical wavelengths for nitrogen, helium, water, and ethyl alcohol are tabulated in the following table (from ref. 17):

Fluid	Critical wavelength, $\lambda_c = 2\pi l$	
	in.	cm
Nitrogen	0.269	0.674
Helium	.068	.173
Water	.660	1.68
Ethyl alcohol	.379	.962

Figure 3 and the film supplement C-263 available on loan and described at the back of this report and in appendix H illustrate how the vapor flow patterns change as a function of diameter. Sphere size is one of the parameters comprising Bond number

$$Bo = \frac{(\rho_l - \rho)R_o^2 g}{\sigma g_c}$$

Thus, for a given fluid, an increase in sphere size increases Bond number. It is evident from the motion picture (film supplement), and also figure 3, that as Bond number is increased beyond $\lambda_c/D = 1$, surface capillary waves appear, signaling the onset of transition. In the transition region, the flow is pseudolaminar (see appendix G). As the waves become undamped, multiple domes appear over the surface (fig. 3, $l/D = 0.19$). It is clear that the single-dome boundary condition breaks down and the single-dome conduction region is replaced by a multidome film-boiling regime. This change leads to the large-Bond-number or multiple-dome model as sketched in figure 7. Because of the randomness of the bubbles in this regime and the magnitude of the Rayleigh number, the heat transfer may be considered turbulent; however, as shown in appendix D, Bond number enters as a parameter, and thus the laminar equations can be used to predict heat transfer (see also refs. 4 and 5).

The data of figure 5 are replotted as a function of $1/Bo_D$ in figure 12. The theoretical line of equation (33) encompasses the helium data and part of the nitrogen data. The nitrogen data for 1-inch- (2.54-cm-) diameter spheres (ref. 16) lies between 7 and 28 percent above the theoretical line. However, major data trends apparently follow, as predicted by equation (33), and it would seem that Bo is a valid parameter.

The data, other than that for helium, also tend to follow the empirical 1/3-power rule, which may or may not be valid for larger- or smaller-diameter spheres than tested. The arguments which lead to the 1/3-power rule were based on the lack of an effect of geometry on the data (ref. 6). At large Bond numbers, the effect of geometry should be small, as predicted by equation (33); moreover, the data of figure 11 indicate that the

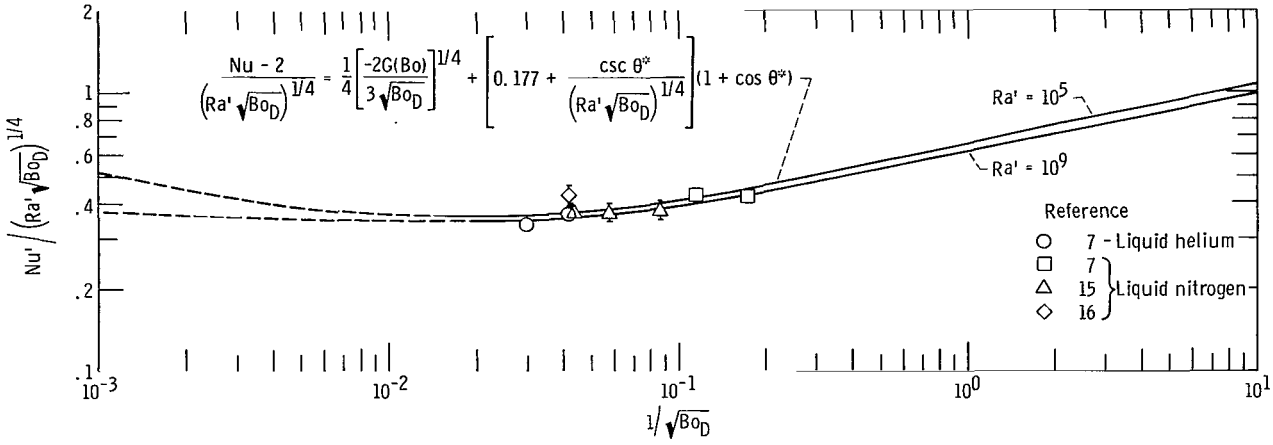

Figure 12. - Experimental and predicted results for film boiling off submerged spheres.

1/4-power rule is valid for high-temperature-difference film boiling. Thus, equation (33) should be valid over a wide range of submerged-sphere film boiling.

CONCLUSIONS

Laminar film-boiling heat transfer on a sphere has been analyzed subject to the optimum entropy production constraint for a large range of Bond numbers. The following results were obtained:

1. The heat-transfer coefficients for film boiling from submerged spheres, as predicted by equation (33), are in fair agreement with the experimental data. Equation (33) represents a linear combination of the low-Bond-number case (single vapor domes) and the high-Bond-number case (multiple vapor domes). For a specific fluid at its normal boiling point, Bond number varies as the square of the sphere radius.

2. No comparison of theory and experiment could be made at very low Bond numbers because of the lack of data. Thus, more experimental data, particularly in the low-Bond-number regime (small spheres) are required before a conclusion can be made as to the validity of the models leading to equation (33). Experimental data at elevated pressures near the critical point and/or at high- or low-gravity conditions would also prove useful.

3. The nonperiodic nature of the interface at the higher Bond numbers is clearly evident in the film supplement. This randomness raised the question as to whether the interface was turbulent or laminar. As the heat-transfer coefficient can be calculated by equation (33), heat transport by the vapor is apparently laminar. Thus, in a turbulent-looking process, the governing mode of heat transport may still be laminar in nature.

4. In view of the interface motion at the higher Bond numbers, the interface velocity boundary condition was changed from nonslip to slip. The data appeared to be bounded between the theoretical nonslip and slip lines; however, the shifts in level within these bounds were unexplainable except through the models leading to equation (33).

5. A motion-picture supplement is offered which compares film boiling from plates, vertical and horizontal, cylinders and spheres.

Before a conclusion can be made as to the validity of the analysis at very small Bond numbers, much more film-boiling data on spheres is required.

Lewis Research Center,
National Aeronautics and Space Administration,
Cleveland, Ohio, February 11, 1969,
129-01-05-17-22.

APPENDIX A

SYMBOLS

A	surface area
a	constant (see eq. (4))
Bo	Bond number based on radius, $g(\rho_l - \rho)R_o^2/\sigma g_c$
Bo_D	Bond number based on diameter, 4 Bo
C	constant, eq. (4)
^3C	constant defined by eq. (C4)
C_p	specific heat of vapor
$C_{1, 2, 3, 4}$	constants
Co	integration constant, eq. (B62)
Co_{opt}	optimization constant
D	diameter
E^2	operator defined by eq. (B15)
F	function defined by eq. (B32)
F_o	function defined by eq. (4)
F_1	function defined by eq. (B65)
F_2	function defined by eq. (B18)
G(Bo)	optimization function, eq. (B64)
G_R	function defined by eq. (B34), $\rho(\rho_l - \rho)gD^3/\mu^2$
g	acceleration of local gravity
g_c	gravitational constant in Newton's law of motion
H*	modified latent heat of vaporization, $\lambda\left(1 + \frac{0.34C_p\Delta T}{\lambda}\right)^2$, see fig. 1
h	heat-transfer coefficient
I_1	nondimensional component of force
k	thermal conductivity
L_o	transition length

l	dome size parameter, $\sqrt{\frac{\sigma g_c}{(\rho_l - \rho)g}} = \frac{\lambda_c}{2\pi}$
Nu	Nusselt number
Nu_{R_o}	Nusselt number based on radius of sphere
Nu'	modified Nusselt number, eq. (B56), $2(\overline{Nu}_{R_o} - 1)$
P	total pressure
P_d	pressure in vapor dome
P_o	environmental pressure
Pr	Prandtl number
p	dimensionless pressure
R_d	radius of vapor dome
R_o	radius of sphere
Ra	Rayleigh number, $G_R Pr$
Ra'	modified Rayleigh number, $Ra \frac{\lambda^*}{C_p \Delta T}$
Re	Reynolds number
Re*	Reynolds number (appendix G), $\frac{y^* u^+ \rho}{\mu}$
r	radial coordinate
S	property group defined by eq. (B45)
T	temperature
ΔT	temperature difference between heater wall and saturation
$\overline{T}_w$	sphere temperature
T_f	film temperature, $(\overline{T}_w + T_s)/2$
T_s	saturation temperature of liquid
u^*	dimensionless velocity defined by eq. (B4)
u^+	velocity at transition, laminar to turbulent
V_r	radial velocity component
V_θ	theta velocity component

v	dimensionless velocity
w	factor defined by eq. (B36)
w^*	nondimensionalizing factor defined by eq. (B37)
y^*	length parameter
α	matching parameter
β	parameter defined by eq. (D11)
γ	coefficient of dome size, see fig. 5 and eq. (B50)
Δ	dimensionless gap thickness defined by eq. (B25)
δ	gap thickness
ζ	dimensionless radial coordinate, see eq. (B1)
Θ	dimensionless temperature defined by eq. (B39)
θ	angular coordinate, see fig. 4
θ^*	angular coordinate at vapor dome, see fig. 4
κ	thermal diffusivity
λ	latent heat of vaporization
λ^*	modified latent heat of vaporization ($\lambda + 0.5C_p\Delta T$)
λ_1^*	modified latent heat of vaporization ($\lambda + 0.4C_p\Delta T$)
λ_c	critical wavelength, $2\pi\sqrt{\frac{\sigma g_c}{(\rho_l - \rho)g}}$
μ	viscosity
ν	kinematic viscosity, μ/ρ
ρ	density of vapor
ρ_l	density of liquid
σ	surface tension
Φ	angular coordinate, see fig. 5
φ	dimensionless function defined by eq. (B29)
ψ	stream function

Subscripts:

cond	conduction

D	diameter
d	dome
exp	experimental
fb	film boiling
fp	flat plate
l	liquid
max	maximum
md	most dangerous
opt	optimum
r	radial direction
t	total
θ	θ direction
1	film boiling
2	film boiling from a flat plate

Superscripts:

—	average value
'	derivative with respect to independent variable

APPENDIX B

METHOD OF SOLUTION

In this appendix, the analytical solutions for the thickness of the thin vapor film and the temperatures, velocity, and pressure profiles within this film are determined. These parameters govern the heat transfer across the thin vapor film. A flow chart of the solution appears as figure 13, and frequent reference to this figure will prove fruitful.

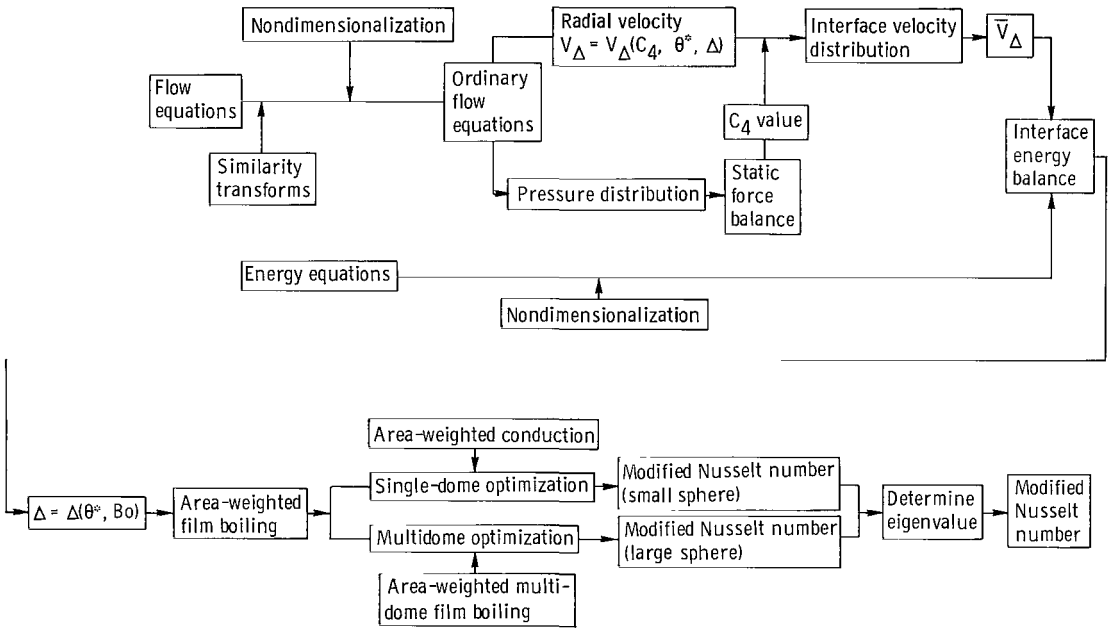

Figure 13. - Solution flow chart.

Momentum Equations

The governing equations (eqs. (9) to (13)) are made nondimensional to generalize the solution by selecting the following parameters:

$$\zeta = \frac{r}{R_o} \tag{B1}$$

$$v_\zeta = \frac{V_r}{u^*} \tag{B2}$$

$$v_\theta = \frac{V_\theta}{u^*} \tag{B3}$$

$$u^* = \frac{\nu}{R_o} \tag{B4}$$

$$R_e = \frac{\rho u^* R_o}{\mu} \equiv 1 \tag{B5}$$

$$p = \frac{P}{\frac{\rho u^{*2}}{g_c}} \tag{B6}$$

Substituting these parameters into the momentum equations (eqs. (9) and (10)) gives

$$0 = -\frac{\partial p}{\partial \zeta} + \nabla^2 v_\zeta - \frac{2}{\zeta^2} v_\zeta - \frac{2}{\zeta^2}\frac{\partial v_\theta}{\partial \theta} - \frac{2}{\zeta^2} v_\theta \cot\theta \tag{B7}$$

$$0 = -\frac{1}{\zeta}\frac{\partial p}{\partial \theta} + \nabla^2 v_\theta + \frac{2}{\zeta^2}\frac{\partial v_\zeta}{\partial \theta} - \frac{v_\theta}{\zeta^2 \sin^2\theta} \tag{B8}$$

where

$$\nabla^2 = \frac{1}{\zeta^2}\frac{\partial}{\partial \zeta}\left(\zeta^2 \frac{\partial}{\partial \zeta}\right) + \frac{1}{\zeta^2 \sin\theta}\frac{\partial}{\partial \theta}\left(\sin\theta \frac{\partial}{\partial \theta}\right) \tag{B9}$$

Introducing the stream function for spherical coordinates (ref. 12, p. 131) gives for the velocity distribution

$$v_r = -\frac{1}{r^2 \sin\theta}\frac{\partial \psi}{\partial \theta} \tag{B10}$$

$$v_\theta = \frac{1}{r \sin \theta} \frac{\partial \psi}{\partial r} \tag{B11}$$

or, in terms of the dimensionless velocities,

$$v_\zeta = - \frac{1}{\zeta^2 \sin \theta} \frac{\partial \psi(\zeta, \theta)}{\partial \theta} \tag{B12}$$

$$v_\theta = \frac{1}{\zeta \sin \theta} \frac{\partial \psi(\zeta, \theta)}{\partial \zeta} \tag{B13}$$

Substituting equations (B12) and (B13) into the momentum equations (eqs. (B8) and (B7)) and combining to eliminate the pressure terms gives

$$E^4(\psi) = 0 \tag{B14}$$

where

$$E^2 \equiv \frac{\partial^2}{\partial \zeta^2} + \frac{\sin \theta}{\zeta^2} \frac{\partial}{\partial \theta} \left(\frac{1}{\sin \theta} \frac{\partial}{\partial \theta} \right) \tag{B15}$$

The similarity transform

$$\psi(\zeta, \theta) = F_2(\zeta)(1 - \cos \theta) \tag{B16}$$

is used to convert equation (B14) into an ordinary differential equation. This type of transformation has been used for solving for flow around a sphere (ref. 17, p. 217). Substituting equation (B16) into equation (B14) yields

$$F_2^4(\zeta) = 0 \tag{B17}$$

This is a linear homogeneous equation of fourth order, the solution of which is

$$F_2(\zeta) = C_1 + C_2 \zeta + C_3 \zeta^2 + C_4 \zeta^3 \tag{B18}$$

Therefore,

$$v_\zeta = -\frac{F_2}{\zeta^2} \tag{B19}$$

$$v_\theta = \frac{F_2' \tan\left(\frac{\theta}{2}\right)}{\zeta} \tag{B20}$$

The constants in the previous equations must be determined from the boundary conditions (eqs. (14) and (15)). In terms of the dimensionless variables, these boundary conditions become

$$v_\theta(1, \theta) = 0 \tag{B21}$$

$$v_\theta(1 + \Delta, \theta) = 0 \tag{B22}$$

$$v_\zeta(1, \theta) = 0 \tag{B23}$$

$$v_\zeta(1 + \Delta, \theta) = v_\Delta \tag{B24}$$

where

$$\Delta \equiv \frac{\delta}{R_o} \tag{B25}$$

Applying these conditions to equations (B19) and (B20) allows the four constants to be expressed in terms of one constant of integration.

$$C_1 = \frac{C_4}{2}(1 - 3\varphi) \tag{B26}$$

$$C_2 = 3C_4\varphi \tag{B27}$$

$$C_3 = -\frac{3C_4}{2}(1 + \varphi) \tag{B28}$$

where

$$\varphi = 1 + \Delta \tag{B29}$$

The dimensionless gap thickness Δ is assumed at this time to be an unknown constant. However, as is shown later in this appendix, this requires that the interface energy balance be satisfied on an average over the heating surface rather than at every point.

The constant C_4 can be found by satisfying the static force balance constraint. First, however, the pressure distribution in the vapor gap must be found. Substituting equations (B19) and (B20) into equations (B7) and (B8) and solving for the pressure distribution gives

$$p(\zeta, \theta) = \frac{2C_3}{\zeta} - 6C_4 \ln \zeta + 12C_4 \ln \left(\sec \frac{\theta}{2}\right) + {}^3C \tag{B30}$$

where C_3 is related to C_4 by equation (B28).

The constants C_4 and ${}^3C$ are determined from the static pressure balance in appendix C in terms of the parameters θ^* and Bo; thus, for $\varphi = 1$,

$$C_4 = \frac{G_R F(\theta^*, \mathrm{Bo})}{3 \times 2^6} \tag{B31}$$

$$F(\theta^*, \mathrm{Bo}) = \frac{\dfrac{4(1 - \sin \theta^*)}{\mathrm{Bo} \sin \theta^*} - (1 - \cos \theta^* + 2 \sin \theta^*)}{\ln \cos^2 \dfrac{\theta^*}{2} + \sin^2 \dfrac{\theta^*}{2}} (\cos \theta^* - 1) \tag{B32}$$

$${}^3C = p_o + \frac{G_R}{8} \left(\frac{2}{\mathrm{Bo} \sin \theta^*} + \frac{\rho}{\rho_l - \rho} \sin \theta^* \right) - 2C_3 + 6C_4 \ln \varphi - 12C_4 \ln \left(\sec \frac{\theta^*}{2}\right) \tag{B33}$$

where

$$G_R = \frac{\rho(\rho_l - \rho) g D^3}{\mu^2} = \frac{6w}{\pi w^*} \tag{B34}$$

$$Bo = \frac{g(\rho_l - \rho)R_o^2}{\sigma g_c} \tag{B35}$$

$$w = \frac{4\pi}{3}(\rho_l - \rho)R_o^3 \frac{g}{g_c} \tag{B36}$$

$$w^* = \frac{\rho u^{*2} R_o^2}{g_c} \tag{B37}$$

Therefore, substituting the constant C_4 in C_1, C_2, and C_3, the velocity and pressure distributions are known relations in φ and θ^*, with Bo as a parameter, where $\varphi = 1 + \Delta$.

Next, the energy equation is considered. Afterwards, the solutions to the energy and momentum equations are combined in the interface energy balance to obtain a solution for the heat-transfer coefficient in terms of θ^*, with Bo as a parameter.

Energy Equation

The nondimensional form of the energy equation (eq. 12) becomes

$$\frac{\partial}{\partial \zeta}\left(\zeta^2 \frac{\partial \Theta}{\partial \zeta}\right) = 0 \tag{B38}$$

where

$$\Theta = \frac{T - \overline{T}_w}{T_s - \overline{T}_w} \tag{B39}$$

Equation (B39) can be solved directly and, when the boundary conditions (eqs. (14) and (15)) are used, yields

$$\Theta = \frac{\varphi}{\Delta}\left(1 - \frac{1}{\zeta}\right) \tag{B40}$$

The temperature gradient at each surface becomes

$$\left.\frac{\partial \Theta}{\partial \zeta}\right|_{\zeta=1} = \frac{\varphi}{\Delta} \tag{B41}$$

$$\left.\frac{\partial \Theta}{\partial \zeta}\right|_{\zeta=1+\Delta} = \frac{1}{\varphi\Delta} \tag{B42}$$

Interface Energy Balance

The velocity and temperature distributions have been expressed, up to this point, in terms of an unknown parameter, the dimensionless vapor gap thickness Δ. The interface energy balance (eq. (20)) is now used to determine the value of this parameter.

First, the radial velocity at the interface must be determined. Substituting the values of the constants C_1 to C_3 into equation (B19) and evaluating the velocity at the interface ($\zeta = 1 + \Delta$) gives

$$\frac{v_\zeta(\varphi, \theta)}{C_4} = \frac{v_\Delta}{C_4} = -\frac{1}{2}\left(\frac{1 - 3\varphi}{\varphi^2} + 3 - \varphi\right) \tag{B43}$$

where C_4 is a function of θ^* and the parameter Bo (see eq. (B31)).

Nondimensionalizing equation (20) results in the interface energy balance

$$v_\Delta = -S \left.\frac{\partial \Theta}{\partial \zeta}\right|_{\zeta=1+\Delta} \tag{B44}$$

where

$$S = \frac{1}{Pr}\left[\frac{C_p\left(\overline{T}_w - T_s\right)}{\lambda^*}\right] \tag{B45}$$

and λ has been replaced by λ^* (see assumption 9 and eq. (3)).

Substituting the expression for v_Δ from equation (B43) into equation (B44) along with the expression for the gradient (eq. (B42) and solving for Δ with $\varphi \approx 1$, gives

$$\Delta^4 = -\frac{2\varphi S}{C_4(\theta^*, Bo)} = \left[-4^4 \frac{3}{2Ra' F(\theta^*, Bo)}\right] \tag{B46}$$

The problem has been reduced to one of determining θ^*.

Now the analytical solution for the total heat transfer through the thin vapor film and the single vapor dome is developed. The heat transport through the vapor dome and the thin vapor film (film boiling) will be area-weighted, and the maximization principle will provide θ^* as a function of Bond number for the low-Bond-number case.

The heat-transfer coefficient and Nusselt number can be constructed from the momentum and energy solutions with θ^* as a parameter.

The heat-transfer coefficient to the sphere is defined as

$$h(\overline{T}_w - T_s) = -k \left.\frac{\partial T}{\partial r}\right|_{r=R_o} \tag{B47}$$

or, in nondimensional form,

$$Nu_{R_o} = \frac{hR_o}{k} = \left.\frac{\partial \Theta}{\partial \zeta}\right|_{\zeta=1} \tag{B48}$$

Substituting equation (B41) into equation (B48) gives

$$Nu_{R_o} = \frac{\varphi}{\Delta} = 1 + \frac{1}{\Delta} \tag{B49}$$

This equation represents the Nusselt number for heat conduction in the thin vapor layer beneath the sphere ($\theta < \theta^*$).

Approximation for Heat Conduction Through Upper Sphere

The vapor dome may be roughly approximated by concentric spheres of radius Ro and $(R_o + \gamma R_o \varphi \sin \theta^*)$, as shown in figure 5. The approximation for $\overline{\Delta}$, shown by the dashed line in figure 5, is

$$\overline{\Delta} = R_o \gamma \varphi \sin \theta^* \tag{B50}$$

where γ is a constant to be discussed in detail in appendix E. Substituting equation (B50) into the right side of equation (B49) gives

$$\left(Nu_{R_o}\right)_{cond} = 1 + \frac{R_o}{\gamma R_o \varphi \sin \theta^*} \tag{B51}$$

The average Nusselt number for the sphere follows as the linear sum of the area-weighted film-boiling and conduction Nusselt numbers.

0

$$\overline{Nu}_{R_o} = \left[Nu_{R_o} \frac{A(\theta \leq \theta^*)}{A_t}\right]_{fb} + \left[\left(Nu_{R_o}\right)_{cond} \frac{A(\theta > \theta^*)}{A_t}\right]_{cond} \tag{B52}$$

The fraction of the surface area in film boiling for a given θ^* can be found directly by integration:

$$x = \frac{\int_0^{2\pi} \int_0^{\theta^*} dA}{\int_0^{2\pi} \int_0^{\pi} dA} = \frac{1 - \cos \theta^*}{2} \tag{B53}$$

The conduction area then is, of course,

$$A_{cond}(\theta > \theta^*) = (1 - x)A_t \tag{B54}$$

When equations (B49), (B51), and (B53) are substituted into equation (B52), the average Nusselt number becomes

$$\overline{Nu}_{R_o} = \left[\left(\frac{1 - \cos \theta^*}{2}\right)\frac{\varphi}{\Delta}\right]_{fb} + \left[\left(\frac{1 + \cos \theta^*}{2}\right)\left(1 + \frac{1}{\gamma \varphi \sin \theta^*}\right)\right]_{cond} \tag{B55}$$

Rearranging yields

$$Nu' = 2\left(\overline{Nu}_{R_o} - 1\right) = \frac{1 - \cos \theta^*}{\Delta} + \frac{(1 + \cos \theta^*)\csc \theta^*}{\varphi \gamma} \tag{B56}$$

Substituting the value of Δ from equation (B46) and assuming $\varphi \approx 1$ yields the following form of equation (B56):

$$Nu' = \frac{1 - \cos\theta^*}{4}\left[\frac{-2Ra'}{3}F(\theta^*, Bo)\right]^{1/4} + (1 + \cos\theta^*)\gamma^{-1}\csc\theta^* \tag{B57}$$

This expression is a function of θ^* and Bo. As Bo is dependent on the type of evaporative fluid and geometry, in any given experiment, the unknowns are reduced to θ^* alone.

To determine θ^*, we apply the optimization criterion to Nu'. For the case of a fixed geometry and constant properties, this criterion may be written as

$$\left.\begin{aligned} D_{\theta^*} Nu' &= 0 \\ D^2_{\theta^*} Nu' &< 0 \end{aligned}\right\} \tag{B58}$$

Differentiating Nu' and equating to zero gives the differential equation

$$\frac{1}{4}D_{\theta^*}\ln\left|-F(\theta^*, Bo)\right| + \frac{\sin\theta^*}{1 - \cos\theta^*} - \frac{\left\{\frac{1}{4}\left[\frac{-2Ra'}{3}F(\theta^*, Bo)\right]^{1/4}\right\}^{-1}}{(1 - \cos\theta^*)^2\gamma} = 0 \tag{B59}$$

Note that the last term in equation (B59) may be rewritten by using equation (B46) as

$$\frac{\Delta}{(1 - \cos\theta^*)^2\gamma} \tag{B60}$$

However, we have assumed Δ to be small, so equation (B59) reduces to

$$D_{\theta^*}\ln\left|-F(\theta^*, Bo)\right| + \frac{4\sin\theta^*}{1 - \cos\theta^*} = 0 \tag{B61}$$

where θ^* is not equal to or greater than π. Rather than complete the above differentiation, equation (B61) can be integrated directly to give

$$F(1 - \cos\theta^*)^4 = Co \tag{B62}$$

which gives a value for θ^* that maximizes the Nusselt number according to equation (B58). Here Co is a constant of integration which represents the locus of boundary conditions determined by the interrelation of θ^* and Bo.

Substituting equation (B62) back into equation (B57) gives

$$Nu' = \frac{1}{4}\left(\frac{-2CoRa'}{3}\right)^{1/4} + (1 + \cos\theta^*)\gamma^{-1}\csc\theta^* \tag{B63}$$

The optimum (or maximum) Nusselt number now depends on Co, θ^*, and Ra'. The maximum values of Co can be determined by solving equation (B62) and plotting Co as

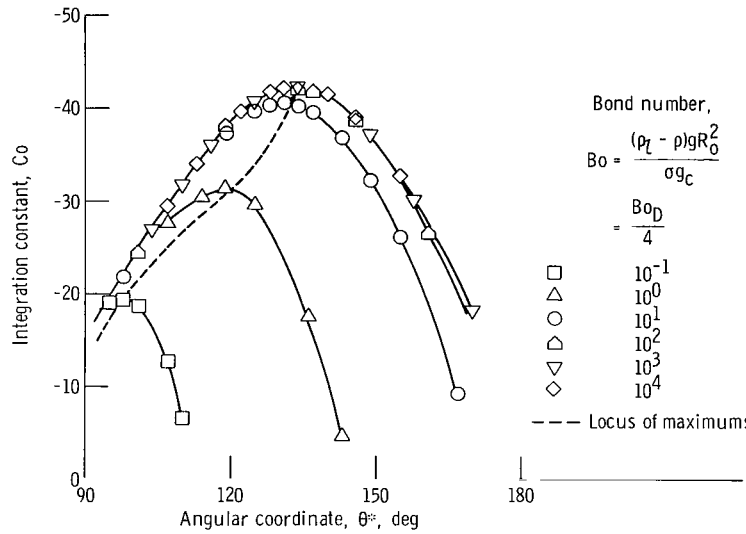

Figure 14. - Families of solutions to $F(1 - \cos\theta^*)^4 = Co$ for various bond numbers and angular coordinate θ^* values.

a function of θ^* for various Bond numbers Bo at a given Ra'. This is illustrated in figure 14, with the dashed line denoting the locus of Co maximums for various Bond numbers at some Ra'. The optimum integration constant Co_{opt} and θ^* values for various Bond numbers are given in figure 6. The locus of Co_{opt} is labeled G(Bo) and is required in the solution of Nu'.

$$Co_{opt} \equiv G(Bo) \tag{B64}$$

Based on these results, the average Nusselt number for the single-dome case becomes

$$Nu' = \frac{1}{4}\left[\frac{-2Ra'G(Bo)}{3}\right]^{1/4} + F_1(Bo) \tag{B65}$$

where G(Bo) and $F_1(Bo) = (1 + \cos\theta^*)\,\gamma^{-1}\csc\theta^*$ are determined from figure 6 for a given Bo. The effect of γ is discussed in appendix E.

APPENDIX C

STATIC PRESSURE BALANCE

The pressure distribution within the vapor gap is obtained directly from the solution to the momentum equations and is repeated here for convenience.

$$p(\zeta, \theta) = \frac{2C_3}{\zeta} - 6C_4 \ln \zeta + 12C_4 \ln \left(\sec \frac{\theta}{2}\right) + {}^3C \tag{B30}$$

where

$$C_3 = -\frac{3C_4}{2}(1 + \varphi) \tag{B28}$$

and ${}^3C$ and C_4 are, as of this point, undetermined constants. In this appendix these constants are determined, using the boundary condition (eq. (17)) and the force balance (eq. (19)), with θ^* and φ as parameters. Figure 15 illustrates the contributing pressure terms.

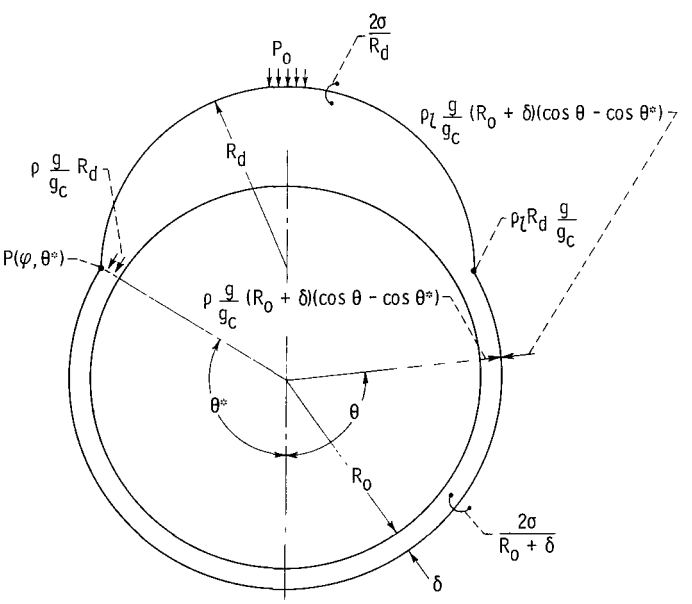

Figure 15. - Schematic of pressure forces acting on sphere.

The pressure in the vapor dome at the exit surface θ^* is, in dimensional terms,

$$P_d = P_o + \frac{2\sigma}{R_d} + \frac{\rho g}{g_c} R_d \tag{C1}$$

where

$$R_d = R_o \varphi \sin \theta^* \tag{C2}$$

The dome pressure P_d represents the sum of the static pressure P_o, the surface-tension pressure difference $(2\sigma/R_o)$, and the vapor head. Therefore, the constant ^3C in equation (B30) may be evaluated as follows:

$$p(\varphi, \theta^*) = \frac{P_d}{\frac{\rho u^{*2}}{g_c}} = \frac{2C_3}{\varphi} - 6C_4 \ln \varphi + 12C_4 \ln \left(\sec \frac{\theta^*}{2}\right) + {}^3C \tag{C3}$$

or

$${}^3C = \left(P_o + \frac{2\sigma}{R_o \varphi \sin \theta^*} + \frac{\rho g R_o \varphi}{g_c} \sin \theta^*\right) \frac{g_c}{\rho u^{*2}} - \frac{2C_3}{\varphi} + 6C_4 \ln \varphi - 12C_4 \ln \left(\sec \frac{\theta^*}{2}\right) \tag{C4}$$

And substituting equation (C4) into equation (B30) yields

$$p(\zeta, \theta) = 2C_3 \left(\frac{1}{\zeta} - \frac{1}{\varphi}\right) - 6C_4 \ln \left(\frac{\zeta}{\varphi}\right) + 12C_4 \ln \left| \frac{\sec \frac{\theta}{2}}{\sec \frac{\theta^*}{2}} \right| + \frac{g_c}{\rho u^{*2}} \left(P_o + \frac{2\sigma}{R_o \varphi \sin \theta^*} + \frac{\rho g}{g_c} R_o \varphi \sin \theta^*\right) \tag{C5}$$

As one of the constraints, the average pressures across the interface must be balanced. Therefore, to evaluate equation (19), we need to establish $\overline{P}$, the average pressure exerted by the liquid upon the interface. The pressure at any point (ζ, θ) becomes

$$P = P_o + \frac{\rho_l R_d g}{g_c} + (R_o + \delta)(\rho_l - \rho)\frac{g}{g_c}(\cos\theta - \cos\theta^*) + \frac{2\sigma}{R_o + \delta} \tag{C6}$$

Total pressure P represents the static head P_o, the liquid head to the base of the vapor dome $\rho_l R_d g/g_c$, the difference in liquid and vapor head to any point below (φ, θ^*), and the pressure drop due to surface tension, which must be balanced by the pressure within the vapor gap. Thus, equation (C6) can be integrated over the sphere to obtain

$$\overline{P} = \frac{\int P\, dA}{\int dA}$$

$$\overline{P} = \frac{\int_0^{\theta^*} (R_o + \delta)^2 \sin\theta \left[P_o + \rho_l R_o \frac{g}{g_c} + (R_o + \delta)(\rho_l - \rho)\frac{g}{g_c}(\cos\theta - \cos\theta^*) + \frac{2\sigma}{R_o + \delta}\right] d\theta}{\int_0^{\theta^*} (R_o + \delta)^2 \sin\theta\, d\theta} \tag{C7}$$

(C8)

For a constant gap thickness and a fixed fluid, equation (C7) becomes

$$\overline{P} = P_o + R_d \rho_l \frac{g}{g_c} + \frac{2\sigma}{R_o + \delta} + \frac{(R_o + \delta)(\rho_l - \rho)\frac{g}{g_c}}{2}(1 - \cos\theta^*) \tag{C9}$$

Integrating the pressure (eq. (C5)) over the sphere gives

$$I_1 = \int_0^{2\pi}\int_0^{\theta^*} p(\varphi,\theta)\varphi^2 \sin\theta\, d\theta\, d\Phi \tag{C10}$$

$$I_1 = 2\pi\varphi^2 \left\{ 12C_4 \left[\ln\left(\cos^2\frac{\theta^*}{2}\right) - \cos^2\frac{\theta^*}{2} + 1 \right] + \frac{(1 - \cos\theta^*)}{\frac{\rho u^{*2}}{g_c}} \left(P_o + \frac{\rho g}{g_c} R_o \varphi \sin\theta^* + \frac{2\sigma}{R_o \varphi \sin\theta^*} \right) \right\} \tag{C11}$$

But by equation (19)

$$\int_A \frac{\overline{P}}{\frac{\rho u^{*2}}{g_c}} \varphi^2 \sin\theta \, d\theta \, d\Phi = I_1 \tag{C12}$$

Substituting equations (C9) and (C11) into equation (C12) and integrating gives

$$12C_4\left(\ln\cos^2\frac{\theta^*}{2} + \sin^2\frac{\theta^*}{2}\right) = \frac{\cos\theta^* - 1}{\frac{\rho u^{*2}}{g_c}}\left[\frac{2\sigma}{R_o\varphi\sin\theta^*}(1 - \sin\theta^*)\right]$$

$$- (\rho_l - \rho)\frac{g}{g_c}R_o\varphi\sin\theta^* - \frac{1}{2}(\rho_l - \rho)\frac{g}{g_c}R_o\varphi(1 - \cos\theta^*) \tag{C13}$$

Introducing the Bond number Bo

$$Bo = \frac{(\rho_l - \rho)gR_o^2}{\sigma g_c} \tag{B35}$$

the weight of the displaced fluid (sphere alone)

$$w = \frac{4\pi}{3}(\rho_l - \rho)R_o^3\frac{g}{g_c} \tag{B36}$$

$$w^* = \frac{\rho u^{*2}R_o^2}{g_c} \tag{B7}$$

into equation (C13) and solving for C_4 yields

$$C_4 = \frac{w\varphi}{32\pi w^*}(\cos\theta^* - 1)\left[\frac{\frac{4(1 - \sin\theta^*)}{Bo\varphi^2\sin\theta^*} - (1 - \cos\theta^* + 2\sin\theta^*)}{\ln\cos^2\frac{\theta^*}{2} + \sin^2\frac{\theta^*}{2}}\right] \tag{C14}$$

$$C_4 = \frac{w\varphi}{32\pi w^*} F(Bo\varphi^2, \theta^*) = \frac{G_R F(\theta^*, Bo\varphi^2)}{3\times 2^6} \qquad \text{(C15)}$$

Thus, C_4 remains a function of Bo, θ^*, and the gap thickness $\varphi = 1 + \Delta$ to be determined by other conditions.

APPENDIX D

LARGE-SPHERE MODIFICATION

In this appendix, the large-Bond-number (large sphere) case is considered. The single dome is replaced by a multiple-dome region, and the basic assumptions are delineated. Then, the overall heat transfer through the thin film and the multiple-dome region is determined. The two regions are area-weighted, and the maximization principle is applied to give θ^* as a function of Bond number and a matching parameter. An equation for heat transfer from large-Bond-number spheres is presented in the form

$$h_{large} = h_1 \frac{A_1}{A_t} + \alpha h_{fp} \frac{A_2}{A_t} \tag{D1}$$

= (Film boiling (transport across thin vapor film, part 1)) + (Film boiling from upward-facing flat plate (transport through multiple-dome region))

where α is an eigenvalue or matching parameter.

Film boiling from a large sphere is modeled in figure 7. In solving the large-sphere regime for the optimum heat-transfer coefficient (or, equivalently, for the Nusselt number), the following assumptions are made:

(1) Flow from the lower stagnation region to the multiple-dome region is described as in the single-dome regime. The solutions of the momentum and energy equations are assumed to be valid to the point of optimization of the heat-transfer coefficient which determines $\theta^* = \theta^*(Bo)$.

(2) The conduction region of the single-dome model is replaced by a multiple-dome film-boiling regime. The heat-transfer coefficient in this region is proportional to that for a flat plate facing upward; the determination of the constant of proportionality in optimizing the heat-transfer coefficient leads to an eigenvalue problem.

(3) The heat transfer may be expressed as a area-weighted sum of the heat transfer in the lower film-boiling region ($\theta < \theta^*$ in fig. 7) and film boiling off the upper portion of the sphere ($\theta > \theta^*$ as described in assumptions (1) and (4)):

$$\frac{Nu'}{2} = Nu_1 \frac{A_1}{A_t} + Nu_2 \frac{A_2}{A_t} \tag{D2}$$

where the Nusselt number for boiling off the lower portion of the sphere is

$$Nu' = Nu - 2 \tag{D3}$$

with

$$Nu_1 = \frac{\varphi}{\Delta} \tag{D4}$$

and

$$\frac{A_1}{A_t} = \frac{1 - \cos \theta^*}{2} \tag{D5}$$

For the top of the sphere,

$$Nu_2 = \alpha \left(\frac{Ra' \sqrt{Bo}}{\pi} \right)^{1/4} \tag{D6}$$

and

$$\frac{A_2}{A_t} = \frac{1 + \cos \theta^*}{2} \tag{D7}$$

and α represents an eigenvalue or matching parameter, to be determined in matching the small- and large-sphere regions, as $(R\theta^*/\lambda_c) \to 1$. Note, a factor of 1/2 was introduced in the left side of equation (D2) so that the Nusselt number would be based on diameter (see eqs. (B55) and (B56)).

(4) The ratio of vapor gap thickness to sphere radius Δ is assumed to be sufficiently small that $\varphi = 1 + \Delta \approx 1$. At this point, it is helpful to consult figure 13 to determine the cause of subsequent events. Equation (D2) may be rewritten as

$$Nu' = \frac{1 - \cos \theta^*}{\Delta} + (1 + \cos \theta^*) \left(Ra' \frac{\sqrt{Bo}}{\pi} \right)^{1/4} \alpha \tag{D8}$$

The dimensionless gap thickness Δ may be written as (see eq. (B46))

$$\frac{1}{\Delta} = \left(-\frac{C_4}{2S}\right)^{1/4} = \left[-\frac{wF(\theta^*, Bo)}{2\times S\times 32\pi w^*}\right]^{1/4} = \frac{1}{4}\left[-\frac{2F(\theta^*, Bo)}{3\sqrt{Bo}}\right]^{1/4}\left(Ra'\sqrt{Bo}\right)^{1/4} \tag{D9}$$

Substituting equation (D9) into equation (D8) and factoring out $\left(Ra'\sqrt{Bo}\right)^{1/4}$ gives

$$\frac{Nu'}{\left(Ra'\sqrt{Bo}\right)^{1/4}} = \frac{1 - \cos\theta^*}{4}\left[-\frac{2F(\theta^*, Bo)}{3\sqrt{Bo}}\right]^{1/4} + \left(\frac{2}{3}\right)^{1/4}\frac{\beta}{4}(1 + \cos\theta^*) \tag{D10}$$

where the modified matching parameter β is defined as

$$\beta = 4\left(\frac{3}{2}\right)^{1/4}\frac{\alpha}{\pi^{1/4}} \tag{D11}$$

Equation (D10) will now be optimized with respect to θ^* to give the optimum large-sphere heat-transfer coefficient (equivalently Nusselt number). Differentiating equation (D10) with respect to θ^* yields the characteristic differential equation:

$$D_{\theta^*}\ln\left|-F(\theta^*, Bo)\right| + \frac{4\sin\theta^*}{1 - \cos\theta^*}\left\{1 - \beta\left[\frac{\sqrt{Bo}}{-F(\theta^*, Bo)}\right]^{1/4}\right\} = 0 \tag{D12}$$

In appendix E, the matching parameter is shown to be

$$\frac{\alpha}{\pi^{1/4}} \approx 0.21 \tag{E4}$$

Applying equations (E4) and (D11) to equation (D10) gives an equation applicable to the large-Bond-number case (large sphere)

$$\frac{Nu'}{\left(Ra'\sqrt{Bo}\right)^{1/4}} = \frac{1}{4}\left[\frac{-2G(Bo)}{3\sqrt{Bo}}\right]^{1/4} + 0.21(1 + \cos\theta^*) \tag{D13}$$

APPENDIX E

COMBINED SOLUTION

In appendix B, an analytical solution for film boiling from spheres was found for the low-Bond-number case. In essence it represents an asymptotic case applicable only where the single vapor dome forms over part of the sphere. In appendix D, a semi-analytic solution for film boiling from spheres was determined to within a constant for the large-Bond-number case.

Small-bond-number case:

$$Nu' = \frac{1}{4}\left[\frac{-2}{3} Ra'G(Bo)\right]^{1/4} + (1 + \cos \theta^*)\gamma^{-1} \csc \theta^* \tag{B65}$$

Large-bond-number case:

$$\left(\frac{Nu'}{Ra' \sqrt{Bo}}\right)^{1/4} = \frac{1}{4}\left[\frac{-2G(Bo)}{3\sqrt{Bo}}\right] + \frac{\alpha}{\pi^{1/4}}(1 + \cos \theta^*) \tag{E1}$$

where α is a parameter to be determined.

To determine a Nusselt number applicable to both the large- and small-sphere regimes (large and small Bo), α must be determined such that the solutions match in the transition regime (film supplement and appendix G). Now the matching parameter α is determined by requiring the large- and small-Bond-number solutions to match at $R_o\theta^*/\lambda_c = 1$. Superimposing the small-sphere solution for θ^* as a function of Bo (fig. 7) onto figure 16 indicates that the two solutions are compatible; that is,

$$\frac{R_o\theta^*}{\lambda_c} = 1 \tag{E2}$$

when the modified matching parameter β becomes

$$\beta = 0.93 \tag{E3}$$

and from equation (D11)

$$\frac{\alpha}{\pi^{1/4}} = \left(\frac{\beta}{4}\right)\left(\frac{2}{3}\right)^{1/4} \approx 0.21 \tag{E4}$$

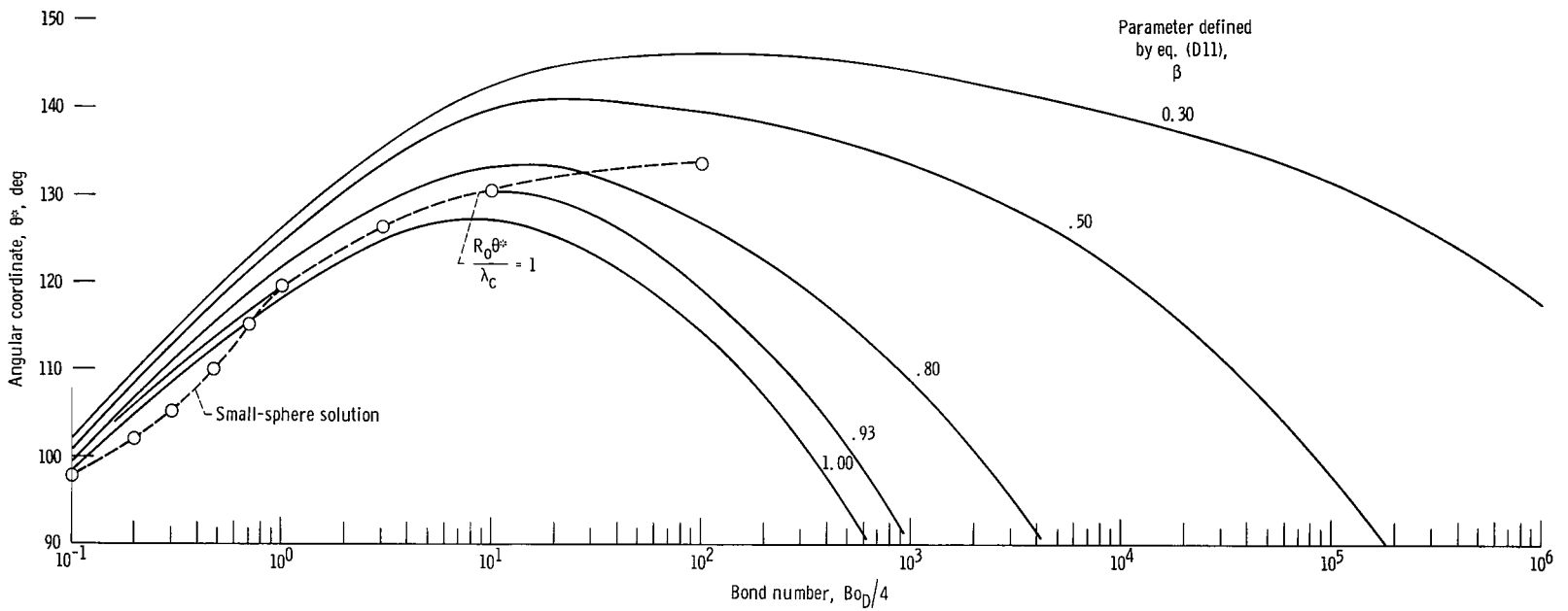

Figure 16. - Large-sphere optimization solution. Locus of angular coordinate θ^* as function of Bond number for several eigenvalues.

A single equation for film boiling off spheres is obtained by forming a linear combination of the large- and small-Bond-number cases (large and small spheres). Linearly combining equations (B65) and (E1) and substituting equation (E4) for $\alpha/\pi^{1/4}$ gives an equation applicable to both large and small Bond numbers

$$\left(\frac{Nu'}{Ra' \sqrt{Bo}}\right)^{1/4} = \frac{1}{4}\left[\frac{-2G(Bo)}{3\sqrt{Bo}}\right]^{1/4} + \left[0.21 + \frac{\csc \theta^* \gamma^{-1}}{\left(Ra' \sqrt{Bo}\right)^{1/4}}\right](1 + \cos \theta^*) \qquad (E5)$$

where $G(Bo)$ and $\theta^* = \theta^*(Bo)$ are determined as functions of Bo from figure 8.

In order to compare the results of this analysis to that of the cylinder and experimental data, it is most expedient to convert equation (E5), in part, to Bond number based on diameter rather than on radius.

$$Bo = \frac{Bo_D}{4} \qquad (E6)$$

Substituting equation (E6) into equation (E5), except for the function $G(Bo)$, results in

$$\frac{Nu'}{\left(Ra' \sqrt{Bo_D}\right)^{1/4}} = \frac{1}{4}\left[\frac{-2G(Bo)}{3\sqrt{Bo_D}}\right]^{1/4} + \left[0.177 + \frac{\csc \theta^* \dfrac{\gamma^{-1}}{4^{1/8}}}{\left(Ra' \sqrt{Bo_D}\right)^{1/4}}\right](1 + \cos \theta^*) \qquad (E7)$$

The expressions for the Nusselt numbers require the evaluation of the constant γ for both the small and large spheres (eq. (B65)) and implicitly for the large sphere (see fig. 7 for single-dome equivalent and fig. 5 for $\overline{\Delta}$). The parameter γ, in effect, determines the average thickness of the vapor dome through which heat is transferred by conduction. This parameter ($\gamma^{-1}/4^{1/8}$) which appears in equation (E7) was assumed to be 1, in agreement with the very large single vapor domes shown in figure 3. With this assumption, equations (B65), (E5), and (E7) become equations (24), (32), and (33), respectively.

APPENDIX F

SLIP CASE

When fluid motion at the interface is present, the problem becomes quite complex; however, when the problem is limited to the single-dome model with slip at the interface, a tractable model results. The boundary conditions are modified as follows:

$$\left.\begin{aligned} &\frac{\partial v_\theta(\varphi,\theta)}{\partial \zeta} = 0 \\ &v_\theta(1,\theta) = 0 \\ &v_\zeta(1,\theta) = 0 \\ &v_\zeta(\varphi,\theta) = v_\Delta \end{aligned}\right\} \tag{F1}$$

As the solution of the governing equations is the same, only the values of the constants, C_1, C_2, C_3, and C_4 change. Substituting equation (F1) into equation (B18) and solving for the constants in terms of C_4 yields

$$C_1 = \frac{C_4}{2}(1 - 3\varphi^2) \tag{F2}$$

$$C_2 = 3\varphi^2 C_4 \tag{F3}$$

$$C_3 = -\frac{3}{2} C_4(1 + \varphi^2) \tag{F4}$$

Using these constants to solve for the interface velocity gives

$$v_\Delta = \frac{C_4 \Delta^3}{2\varphi^2}(3\varphi + 1) \tag{F5}$$

This, of course, alters the magnitude of the interface energy balance over that previously determined for the nonslip case. Using equations (F5) and (B44), the interface energy balance for the slip case is

$$v_{\Delta} = S \left.\frac{\partial \Theta}{2\zeta}\right|_{\zeta=\varphi} = -\frac{S}{\varphi\Delta} \tag{F6}$$

$$= \left(\frac{C_4\Delta^3}{2\varphi^2}\right)(3\varphi + 1) \tag{F7}$$

Solving equations (F6) and (F7) for Δ

$$\Delta^4 = -\left(\frac{2\varphi}{3\varphi + 1}\right)\left(\frac{S}{C_4}\right) \tag{F8}$$

For the situation where φ is approximately 1,

$$\Delta^4 = -\frac{S}{2C_4} \tag{F9}$$

where C_4 is identical with the previous definition of C_4 (eq. (B31)). A comparison of equations (F9) and (B46) lead to a Nusselt number ratio for the slip and nonslip cases:

$$\frac{Nu_{slip}}{Nu_{nonslip}} \propto \left(\frac{\Delta_{nonslip}}{\Delta_{slip}}\right)^{1/4} = \sqrt{2} \tag{F10}$$

Therefore, the slip condition (eq. (B65)) may be written as

$$Nu' = \sqrt{2}\left\{\frac{1}{4}\left[-\frac{2}{3}G(Bo)Ra'\right]^{1/4} + F_1(Bo)\right\} \tag{F11}$$

APPENDIX G

SURFACE WAVES

Hsu (ref. 18) studied film boiling off a vertical flat plate. In order to predict local heat-transfer data, a transition length L_o had to be determined. Hsu assumed that the transition from laminar to turbulent flow occurred at a characteristic Reynolds number of Re* = 100. Knowing Re*, the transition length L_o may be calculated as

$$L_o = \frac{\mu H^* y^*}{2k\Delta T} Re^*$$

where

$$y^* = \left[\frac{2\mu^2 Re^*}{g\rho(\rho_l - \rho)}\right]^{1/4}$$

The variation of L_o with temperature difference is illustrated in figure 17 for two fluids, water and nitrogen. While both fluids may possess minimums, that of nitrogen is quite pronounced near 200 K. This also suggests that the surface becomes more stable near

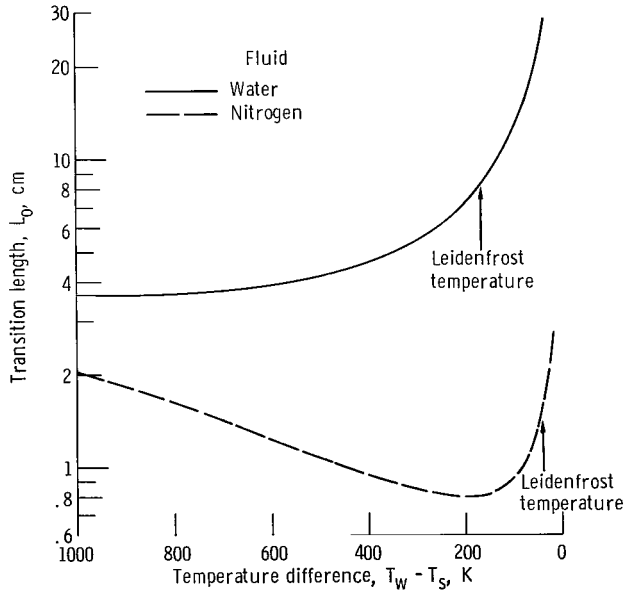

Figure 17. - Critical height for transition to turbulent flow. Theory from reference 3; pressure, 1 atmosphere.

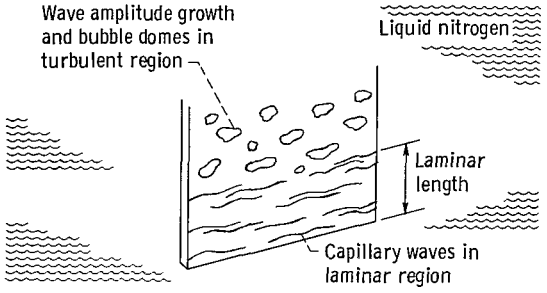

(a) On surface of vertical flat plate.

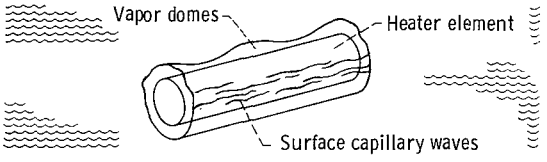

(b) On surface of cylinder.

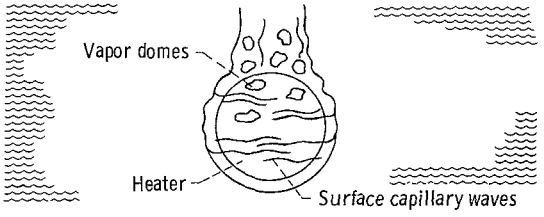

(c) On surface of sphere.

Figure 18. - Illustration of flow profiles.

the Leidenfrost temperature, an observation verified by experiment. Flow on a vertical plate is illustrated in figure 18(a). Note the capillary waves in the laminar region which roll off the bottom of the plate. These waves are most easily demonstrated by the film supplement (available on request).

Some more recent observations of thin films (ref. 19) indicate the existence of several regimes - laminar, pseudolaminar, transition, pseudoturbulent, and turbulent. From these observations, it is evident that $Re^* = 300$ could represent an upper bound to the transition regime or an increase in L_o by $3^{4/3}$.

Thus, for film boiling of nitrogen off a vertical flat plate at a temperature difference of 480 K, L_o would fall in the range $1.02 \leq L_o \leq 4.4$ cm (see fig. 17). Within this length and for some distance beyond, the surface capillary waves and disturbances will not strongly affect the heat transfer (i.e., it remains laminar in nature).

Analogous results are found in film boiling off cylinders, as seen in figure 18(b) and the film supplement. In this case, the heat transfer is predicted in reference 5 with a laminar analysis and by optimizing the heat transfer with respect to a critical wavelength.

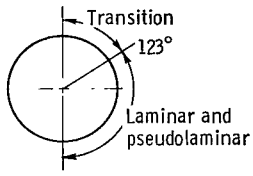

(a) Sphere diameter, 3/8 inch (0.95 cm).

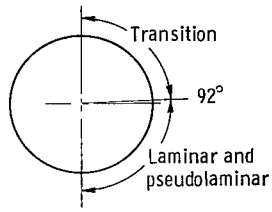

(b) Sphere diameter, 1/2 inch (1.27 cm).

Figure 19. - Laminar, pseudolaminar, and transition regimes for spheres submerged in nitrogen.

Even though the surface appears to be quite turbulent (fig. 2), the heat transport is governed by the laminar equations and the Bond number.

The sphere is no exception. Capillary waves travel over the surface (see fig. 18(c) and the film supplement). At large Bond numbers, the surface appears to be quite turbulent (fig. 3). Pursuing the concept that $R_o\theta$ and L_o are directly related, we can postulate the laminar, pseudolaminar, and transition regimes for spheres submerged in nitrogen (fig. 19).

A comparison of figure 19 and figure 3 indicates some capillary wave activity in the pseudolaminar region, but the waves do not appear to grow. In the transition regimes, however, these waves appear to be growing, and vapor is sometimes sheared off, which forms bubbles.

It is to be concluded that while a process may appear turbulent, the governing character of the heat transport may still be laminar.

APPENDIX H

MOTION-PICTURE SUPPLEMENT - A DESCRIPTION

The motion-picture supplement presents visual observations on film boiling of liquid nitrogen from three different geometries: the flat plate, oriented in the horizontal and vertical positions, a series of horizontal cylinders of different diameters, and a series of spheres of various diameters. The diameters of the cylinders and the spheres are similar to permit comparison of the boiling phenomenon from large and small diameters. The interaction of diameter and interface stability, Bond number, is discussed and illustrated. By changing the size of the cylinder and the sphere, the viewer can visualize the effects of Bond number, see also figure 3. For a more complete discussion of the stability effects, see appendix G.

Effect of Surface Disturbances

For each of these geometries, the relation between small disturbances and a critical wavelength is discussed to determine if the disturbances grow or decay (fig. 20). A stability map which summarizes some essential results of hydrodynamic stability theory is presented as figure 21. If the disturbance wavelength is less than the critical wavelength, the disturbance will decay; however, if the disturbance wavelength is greater than the critical wavelength, it will grow, and an unstable interface results. The wavelength for maximum growth is predicted and labeled the most dangerous wavelength λ_{md}; however, experimental data tend to fall to the right of λ_{md}, as seen on figure 21.

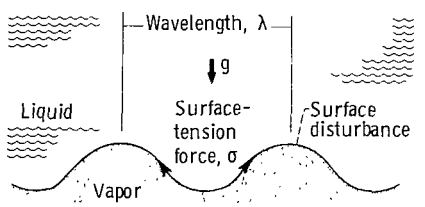

Figure 20. - Surface disturbances related to critical wavelength λ_c: $\lambda < \lambda_c$, disturbance is damped; $\lambda > \lambda_c$, disturbance grows; where $\lambda_c = \sqrt{\frac{\sigma}{(\rho_\ell - \rho)g}}$

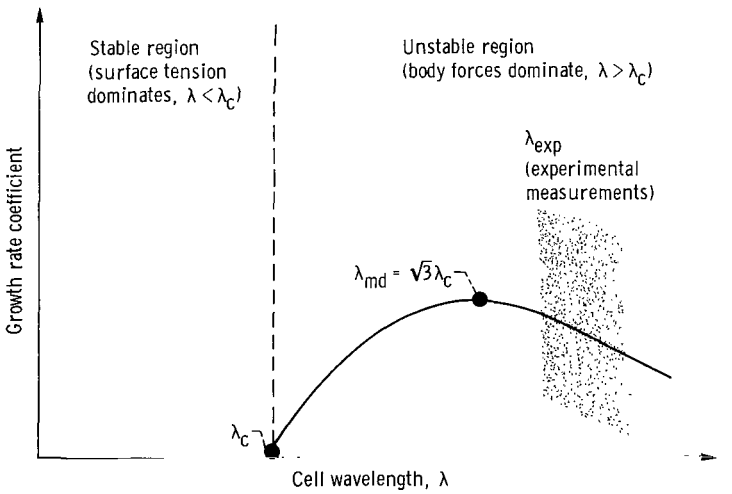

Figure 21. - Stability map.

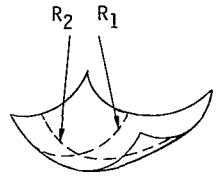

Figure 22. - Gaussian curvature of typical surface element.

Vertical Flat Plate

A surface with no curvature (fig. 22), where $R_1 \to \infty$ and $R_2 \to \infty$, is placed in liquid nitrogen, and the ensuing flow phenomena are photographed. A thin vapor layer quickly forms over the surface and begins to grow. At the first transition point, some instabilities are noted, while at the second transition point, Hsu (ref. 18) notes a significant change in heat-transfer coefficient. This signifies a change to turbulent heat transfer. The observation is quite important because even though the interface is unstable, the heat transport can still be governed by the laminar equations; however, the significant shift in the coefficient at the second transition is irrevocable evidence of a change in mechanism.

Unfortunately, the plate was not instrumented and only the observations of film boiling are available.

Horizontal Flat Plate

While this surface has no curvature, its orientation with respect to the gravity vector changes, which affects the interface geometry. In this case, the interface may be considered to be composed of many vapor domes, as depicted in figure 23. The heat vaporizes the liquid at the interface, and it flows into the vapor domes. These vapor domes, in reality, grow and are released into the fluid reservoir. This action is seen in the motion picture. The multiple domes reach an optimum spacing according to the critical wavelength for the fluid (ref. 13). A periodicity of the vapor domes can be seen in the film.

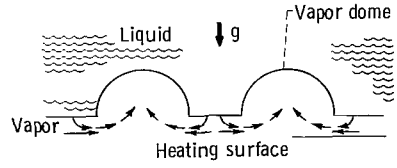

Figure 23. - Model of film boiling from horizontal surface.

Horizontal Cylinder

Here R_1 is finite, however $R_2 \to \infty$. This represents a significant change in geometry. A secondary geometric change is invoked as $R_1 \to \lambda_c/2$; in this regime the basic flow about the cylinder is altered.

Small cylinder. - When $R_1 \ll \lambda_c/2$, the vapor flows parallel to the axis of the cylinder and escapes in a regular periodic manner through vapor domes, as seen in figure 24(a).

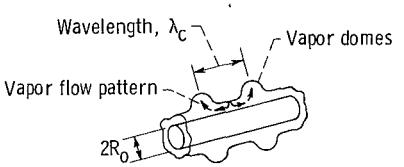

(a) Small.

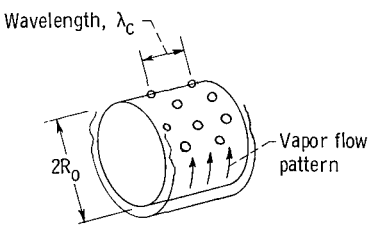

(b) Large.

Figure 24. - Vapor flow patterns for large and small heating cylinders.

Large cylinder. - When $R_1 > \lambda_c/2$, the vapor flows around the cylinder and escapes in a chaotic manner near the upper portion of the cylinder (see fig. 24(b)).

As shown in the main text, the terms large and small are relative to a given fluid; it is the Bond number that determines the regime.

To illustrate the changes in vapor patterns, several different size cylinders were placed in liquid nitrogen and photographed.

Sphere

For this geometry, $R_1 = R_2$. This represents another significant change in geometry. It is apparent from the motion picture and the models presented in this report that there exist large and small sphere regimes analogous to that found for the cylinder. Again,

large and small are relative terms, and it is the Bond number which determines the regime.

Small spheres. - This regime is characterized by a single vapor dome, $R_1 << \lambda_c/2$, forming and departing in a periodic manner. The phenomenon is modeled in figure 5. The motion picture indicates some surface capillary waves even for the single-dome cases, which, for the larger spheres, grow and lead to the multiple-dome regime.

Large spheres. - Many vapor domes appear on the upper portion of the sphere, and the periodicity is dubious ($R_1 > \lambda_c/2$); however, the model (fig. 7) assumes some regularity to form a tractable problem. This was also done for the large cylinder.

To illustrate how the flow patterns change, several different-size spheres were placed in liquid nitrogen and photographed. No heat-transfer data were taken.

In the closing sequence of the film, the flow patterns encompassing the "large" sphere and cylinder are compared; at the same time, the patterns about the "small" sphere and cylinders are compared. Cross comparisons and comparisons between the geometries can also be made.

REFERENCES

1. Bromley, LeRoy A.: Heat Transfer in Stable Film Boiling. Chem. Eng. Progr., vol. 46, no. 5, May 1950, pp. 221-227.

2. Banchero, J. T.; Barker, G. E.; and Boll, R. H.: Stable Film Boiling of Liquid Oxygen Outside Single Horizontal Tubes and Wires. Preprint 3, AIChE Heat Transfer Symposium Annual Meeting, St. Louis, Mo., Dec. 13-16, 1953.

3. Berenson, P. J.: Film-Boiling Heat Transfer from a Horizontal Surface. J. Heat Transfer, vol. 83, no. 3, Aug. 1961, pp. 351-358.

4. Breen, B. P.; and Westwater, J. W.: Effect of Diameter of Horizontal Tubes on Film Boiling Heat Transfer. Chem. Engr. Progr., vol. 58, no. 7, July 1962, pp. 67-72.

5. Baumeister, Kenneth J.; and Hamill, Thomas D.: Laminar Flow Analysis of Film Boiling From a Horizontal Wire. NASA TN D-4035, 1967.

6. Frederking, T. H. K.; and Clark, J. A.: Natural Connection Film Boiling on a Sphere. Advances in Cryogenic Engineering. Vol. 8. K. D. Timmerhaus, ed., Plenum Press, 1963, pp. 501-506.

7. Frederking, T. H. K.; Chapman, R. C.; and Wang, S.: Heat Transport and Fluid Motion During Cooldown of Single Bodies To Low Temperatures. International Advances in Cryogenic Engineering. Vol. 10. K. D. Timmerhaus, ed., Plenum Press, 1965, pp. 353-360.

8. Baumeister, Kenneth J.; Hendricks, Robert C.; and Hamill, Thomas D.: Metastable Leidenfrost States. NASA TN D-3226, 1966.

9. Baumeister, Kenneth J.; and Hamill, Thomas D.: Creeping Flow Solution of the Leidenfrost Phenomenon. NASA TN D-3133, 1965.

10. Baumeister, Kenneth J.; Hamill, Thomas D.; and Schoessow, Glen J.: A Generalized Correlation of Vaporization Times of Drops in Film Boiling on a Flat Plate. Proceedings of the Third International Heat Transfer Conference. Vol. 4. AIChE, 1966, pp. 66-73.

11. Baumeister, K. J.; Hamill, T. D.; Schwartz, F. L.; and Schoessow, G. J.: Film Boiling Heat Transfer to Water Drops on a Flat Plate. Chem. Eng. Progr. Symp. Ser., vol. 62, no. 64, 1966, pp. 52-61.

12. Bird, R. Byron; Stewart, Warren E.; and Lightfoot, Edwin N.: Transport Phenomena. John Wiley & Sons, Inc., 1960.

13. Hamill, Thomas D.; and Baumeister, Kenneth J.: Film Boiling Heat Transfer From a Horizontal Surface As An Optimal Boundary Value Process. Proceedings of the Third International Heat Transfer Conference. Vol. 4. AIChE, 1966, pp. 59-65.

14. Baumeister, K. J.; and Hamill, T. D.: Film Boiling From a Thin Wire as an Optimal Boundary-Value Process. Paper 67-HT-62, ASME, Aug. 1967.

15. Rhea, Lyle Gordon: Boiling Heat Transfer From an Oscillating Sphere With a Cryogenic Fluid at Atmospheric Pressure and Standard Gravity. Ph. D. Thesis, Kansas State University, 1967.

16. Merte, H.; and Clark, J. A.: Boiling Heat-Transfer Data for Liquid Nitrogen at Standard and Near-Zero Gravity. Advances in Cryogenic Engineering. Vol. 7. K. D. Timmerhaus, ed., Plenum Press, 1962, pp. 546-550.

17. Hamielec, A. E.; Hoffman, T. W.; and Ross, L. L.: Numerical Solution of the Navier-Stokes Equation for Flow Past Spheres. I. AIChE J., vol. 13, no. 3, Mar. 1967, pp. 212-219.

18. Hsu, Y. Y.; and Westwater, J. W.: Approximate Theory For Film Boiling on Vertical Surfaces. Chem. Eng. Prog. Symp. Ser., vol. 56, no. 30, 1960, pp. 15-24.

19. Portalski, S.: Studies of Falling Liquid Film Flow-Film Thickness on a Smooth Vertical Plate. Chem. Eng. Sci., vol. 18, Dec. 1963, pp. 787-804.

NATIONAL AERONAUTICS AND SPACE ADMINISTRATION
WASHINGTON, D. C. 20546
OFFICIAL BUSINESS

FIRST CLASS MAIL

POSTAGE AND FEES PAID
NATIONAL AERONAUTICS AND
SPACE ADMINISTRATION

POSTMASTER: If Undeliverable (Section 158 Postal Manual) Do Not Return

"The aeronautical and space activities of the United States shall be conducted so as to contribute . . . to the expansion of human knowledge of phenomena in the atmosphere and space. The Administration shall provide for the widest practicable and appropriate dissemination of information concerning its activities and the results thereof."

—NATIONAL AERONAUTICS AND SPACE ACT OF 1958

NASA SCIENTIFIC AND TECHNICAL PUBLICATIONS

TECHNICAL REPORTS: Scientific and technical information considered important, complete, and a lasting contribution to existing knowledge.

TECHNICAL NOTES: Information less broad in scope but nevertheless of importance as a contribution to existing knowledge.

TECHNICAL MEMORANDUMS: Information receiving limited distribution because of preliminary data, security classification, or other reasons.

CONTRACTOR REPORTS: Scientific and technical information generated under a NASA contract or grant and considered an important contribution to existing knowledge.

TECHNICAL TRANSLATIONS: Information published in a foreign language considered to merit NASA distribution in English.

SPECIAL PUBLICATIONS: Information derived from or of value to NASA activities. Publications include conference proceedings, monographs, data compilations, handbooks, sourcebooks, and special bibliographies.

TECHNOLOGY UTILIZATION PUBLICATIONS: Information on technology used by NASA that may be of particular interest in commercial and other non-aerospace applications. Publications include Tech Briefs, Technology Utilization Reports and Notes, and Technology Surveys.

Details on the availability of these publications may be obtained from:

SCIENTIFIC AND TECHNICAL INFORMATION DIVISION

NATIONAL AERONAUTICS AND SPACE ADMINISTRATION

Washington, D.C. 20546